NASA TECHNICAL NOTE

NASA TN D-4914

NASA TN D-4914

EFFECTS OF STEADY-STATE ACCELERATION ON COMBUSTION CHARACTERISTICS OF AN ALUMINIZED COMPOSITE SOLID PROPELLANT

by G. Burton Northam

Langley Research Center
Langley Station, Hampton, Va.

NATIONAL AERONAUTICS AND SPACE ADMINISTRATION • WASHINGTON, D. C. • DECEMBER 1968

NASA TN D-4914

EFFECTS OF STEADY-STATE ACCELERATION ON COMBUSTION CHARACTERISTICS OF AN ALUMINIZED COMPOSITE SOLID PROPELLANT

By G. Burton Northam

Langley Research Center
Langley Station, Hampton, Va.

NATIONAL AERONAUTICS AND SPACE ADMINISTRATION

For sale by the Clearinghouse for Federal Scientific and Technical Information
Springfield, Virginia 22151 – CFSTI price $3.00

Page Intentionally Left Blank

EFFECTS OF STEADY-STATE ACCELERATION ON COMBUSTION CHARACTERISTICS OF AN ALUMINIZED COMPOSITE SOLID PROPELLANT*

By G. Burton Northam
Langley Research Center

SUMMARY

The objective of this investigation was to determine the effect of (1) acceleration level, and (2) acceleration field orientation on the combustion of aluminized composite solid propellant. Unidirectional burning slab motors (4 in. wide by 6 in. long by 0.5 in. thick (101.6 mm wide by 152.4 mm long by 12.7 mm thick) propellant slab) were fired on a ballistics centrifuge at acceleration levels from 0g to 300g. Tests were conducted with the acceleration loads directed normal into the burning surface, normal out of the burning surface, and at orientations of 0^{o}, 30^{o}, 60^{o}, and 75^{o} into the burning surface. The resulting surface condition of the propellant was examined under the various test conditions by extinguishing a limited number of propellant samples.

As the normal acceleration load into the burning surface increased, the average propellant burning rate, the pitting of the propellant surface, and the amount of "metallic-like" residue retained within the test motor increased. At orientations other than normal and into the burning surface, neither the burning rate, the pitting, nor the metallic-like residue were much increased at acceleration levels as high as 300g. At an average chamber pressure of 500 psia (3.45 MN/m^2) the propellant burning rate increased approximately 21 percent as the normal acceleration level was raised from 0g to 300g. The propellant burning rate was most sensitive to increased acceleration loads at the higher pressure levels. Empirical burning-rate equations including the effects of pressure and normal acceleration level were generated.

INTRODUCTION

The performance characteristics of many solid-propellant rocket motors have proved to be affected by the acceleration loads imposed on the burning propellant during spin-stabilized flight. (See ref. 1.) Figure 1 shows the pressure histories of the

---

*The information presented herein was offered as a thesis in partial fulfillment of the requirements for the degree of Master of Science in Mechanical Engineering, Virginia Polytechnic Institute, Blacksburg, Virginia, June 1965.

Altair I (X-248) rocket motor when tested under static conditions and when flown at a spin rate of 600 rpm (10 rps) at a longitudinal acceleration of approximately 14g. At approximately 22 seconds during the 600 rpm (10 rps) flight, the motor chamber pressure increased substantially above the nominal static-test pressure level.

In order to simulate the radial loads imposed on spin-stabilized rockets, ground-test apparatus capable of spinning full-scale motors about their longitudinal axes during firing have been employed to determine the effects of the centrifugal loading on motor performance. (See ref. 2.) Results found in reference 2 indicate two major effects of spinning on motor performance: (1) increased operating pressure and decreased burning time, and (2) severe chamber heating and the retention of metallic slag within the motor chamber. (See ref. 3.) In figure 2 the effects of severe case heating are shown by the postfiring condition of Altair II (X-258) glass fiber chamber following a ground spin test at 250 rpm (4.17 rps).

Figure 3 shows the pressure histories of the Naval Ordnance Test Station 551 (NOTS 551) rocket motor fired under static, ground spin, and spin-stabilized flight conditions. In this motor, as in several other spin-stabilized motors that have been both spin tested and flown at similar spin rates, the flight environment tended to reduce the effect of the spin-induced radial acceleration. (See ref. 3.)

There appear to be at least two causes for the performance variations experienced by spin-stabilized rockets. At the lower spin rates the effects appear to be due to changes in surface combustion phenomena; whereas at the higher spin rates the presence of a strong vortex contributes to the observed effects.

The ability to incorporate acceleration-induced ballistic effects into the initial motor design would reduce the development cost associated with the cut-and-try techniques presently employed in the design of solid fuel rockets. In order to predict the ballistic and hardware requirements of a rocket motor operating in a spin-stabilized vehicle, the functional relationships between burning rate, chamber pressure, residue weight, acceleration level, and orientation of the burning surface with respect to the acceleration vector must be defined. This paper presents the results obtained from a systematic study of these parameters using a 16-percent aluminized polybutadiene acrylic acid propellant (designated PBAA).

SYMBOLS

a	burning rate constant, inches/second (millimeters/second)
a_n	normal acceleration, g

$\bar{d}$ average diameter, inches (meters)

g gravitational constant, 32.2 feet/second^2 (9.8 meters/second^2)

n pressure exponent in Vieille's equation

p average chamber pressure during web burn time, pounds/square inch absolute (newtons/meter^2)

r propellant burning rate, inches/second (millimeters/second)

r_g propellant burning rate under acceleration environment, inches/second (meters/second)

t_b web burn time, seconds

$\bar{w}$ average residue weight retained on lower insert at a given acceleration level, grams

θ half-angle, degrees

APPARATUS

Centrifuge

The centrifuge used to produce the desired acceleration levels is located at the Langley Research Center. A photograph of the centrifuge is shown in figure 4. The machine is capable of subjecting a 100-pound test specimen to a centrifugal acceleration of 300g. Firing current and other required instrumentation signals were transmitted to the rotating arm through low-noise silver graphite slip rings. (See ref. 4 for a complete description of the test facility.)

Test Motor

In an attempt to minimize the effects of propellant geometry and spin-induced vortex flow so that acceleration effects alone could be investigated, the unidirectional burning slab motor shown in figure 5 was designed. Within the 6-inch-diameter (152.4 mm) pressure vessel were located the upper and lower inserts. The upper insert formed the cavity for a tapered rectangular gas port. The tapered port was used to

provide approximately constant gas velocity along the length of the 4-inch (101.6 mm) wide by 6-inch (152.4 mm) long propellant slab. The 1/2-inch-thick (12.7 mm) propellant slab was inhibited on five sides and bonded to the lower insert with propellant inhibitor material. Converging-diverging axisymmetric nozzles of graphite with different throat diameters were used in order that pressure could be treated as an independent variable. The ignitor contained from 28 to 30 boron potassium nitrate pellets ($BKNO_3$) 0.25 inch (6.35 mm) in diameter located in a 0.375-inch-diameter (9.53 mm) by 4-inch-long (101.6 mm) pellet chamber. Eight 0.125-inch-diameter (3.18 mm) ignitor gas ports exhausted the ignitor gases across the 4-inch (101.6 mm) by 6-inch (152.4 mm) surface of the propellant into the motor chamber. The $BKNO_3$ pellets were ignited by an electrical squib. The motor assembly was mounted at a 45-inch (1.14 m) radius on the ballistics centrifuge.

The centrifuge acceleration loads were applied at different orientations with respect to the burning surface by rotating the inserts within the motor case. At all orientations the acceleration vector was perpendicular to the thrust axis. Figure 6 illustrates the various orientations of the burning surface, and defines the terminology used in the discussion of the results.

Extinction Test Apparatus

A "blow-off" nozzle and a water quench system were employed in order that the propellant could be partially burned under the acceleration conditions, extinguished, and the remaining surface examined for changes due to the acceleration environment. A photograph of the apparatus used for this test is shown in figure 7. The nozzle assembly of the test motor was modified to accept explosive bolts which released the plate that held the graphite throat. Upon the activation of the explosive bolts at the proper time during motor burning, the motor throat area was rapidly increased and a solenoid valve released a small amount of water into the chamber through the ignitor ports to cool the chamber and prevent reignition. To accomplish extinction, it was necessary to replace the 4- by 6-inch (101.6 by 152.4 mm) slab by a 4-inch (101.6 mm) square slab. The removal of this 2-inch (50.8 mm) length of propellant from the ignitor end of the propellant slab was not thought to affect appreciably the results of the extinction tests. A mechanism was designed to retain the nozzle blow-off plate during an extinction test and thus prevent damage to the test facility.

Propellant

A single batch of a conventional aluminized polybutadiene acrylic acid (PBAA) propellant was used for this investigation. This propellant contained approximately 70 percent by weight of ammonium perchlorate (AP). The ratio of unground to ground

ammonium perchlorate in this formulation was 1.86. The ground ammonium perchlorate had an average (by weight) particle size of 12 microns from a particle size distribution as determined by a micromerograph. This distribution is shown in figure 8(a). The unground ammonium perchlorate had an average (by weight) particle size of 200 microns and a particle size distribution (sieve analysis) as shown in figure 8(b). This combination of ammonium perchlorate sizes gave a weighted average particle size for this propellant of 134.2 microns. The propellant contained approximately 16 percent by weight of aluminum with an average particle size of 7 microns and a particle size distribution (micromerograph) as shown in figure 8(c). The propellant contained approximately 14 percent by weight of PBAA binder and cure agent. The physical properties for this propellant batch are as follows:

Secant modulus at 298° K	420 psi (2.90 MN/m^2)
Maximum stress (298° K)	123 psi (0.85 MN/m^2)
Strain at maximum stress	0.293 in./in. (mm/mm)
Density	0.064 lbm/in^3 (1.77 gm/cm^3)

PROCEDURE

The propellant was cast into paper boxes and cured. Propellant slabs slightly greater than the 4- by 6- by 0.5-inch (101.6- by 152.4- by 12.7-mm) desired dimensions were sawed from the cured propellant blocks. The propellant surfaces were trimmed and then sanded to remove the irregularities from the sawing operation. The propellant thickness was then measured with a micrometer to determine the web thickness at three stations along the 6-inch (152.4 mm) center line of the slab. The average of these three readings was used to determine the propellant web thickness that was later used in the burning-rate calculations.

Test Procedure

The assembled motor with the inserts rotated to the desired orientation was mounted on the centrifuge, the ignitor installed, and the instrumentation connected. After the centrifuge machine had been brought to the speed required for the desired acceleration level, the test motor was fired. The thrust of the small test motor had very little effect on the centrifuge speed because of the large moment of inertia of the rotating arm. Also, since the change of radius due to the regression of the burning surface was only 0.5-inch (12.7 mm) at a 45-inch (1.14 meter) radius, the acceleration level was considered to be constant during burning and calculated at the midpoint of the propellant grain. After test motor burnout, the centrifuge was gradually brought to rest. The test motor was disassembled and the inserts examined. Any remaining metallic residue from the lower inserts was collected and analyzed.

The extinction tests were performed in a manner similar to the regular tests, except that at a preprogramed time during motor burning, the explosive bolts and the water control solenoid were electrically activated and thus the motor was extinguished.

Residue Analysis

The metallic-like residue and loose charred liner material were brushed from the lower inserts. In order to separate the metallic residue from the carbon liner material, the residue was brushed through successively smaller sieve screens. This brushing separated the carbon from the metallic residue, the residue being retained by the screens and the carbon crumbling and falling through to the pan. The amount of residue remaining on successive screens was weighed and the screen size recorded. Thus, the residue particle size data were obtained as weight percent retained on the sieves. Limited chemical analyses to determine approximate percentage of aluminum in the residue were performed.

Data Reduction

Two pressure gages located one at each end of the pellet chamber were used to measure chamber pressure through the ignitor ports. The pressure levels were recorded by use of strip chart recorders at a paper speed of approximately 14 inches per second (0.356 meter per second). The strip chart record was reduced and the tabulated pressure history was integrated with a computer. The average burning rate was determined by dividing the average propellant thickness by the motor burning time t_b. The burning time was determined by the generally accepted tangent-bisector method illustrated in figure 9. The average operating pressure during motor burn time was determined by dividing the integrated pressure history by the motor burning time. This figure also shows the pressure histories of motors fired at 0g and at 200g normal accleration. Because of the variation in nozzle area caused by the deposition of condensed combustion products in the nozzle throat, no attempt was made to calculate instantaneous burning rates from the pressure time data. Also, since the extinction tests indicated that the propellant surface area was increased because of pitting under acceleration conditions (this pitting indicated localized increases in liner burning rate), the average burning rate, as defined, was used as a measure of the effects of acceleration on the combustion process.

DISCUSSION OF RESULTS

The investigation revealed several distinct effects of acceleration on the internal ballistic characteristics of the 16-percent aluminized polybutadiene acrylic acid composite propellant tested. The results are presented in three main parts: ballistic effects, residue effects, and extinction test results.

Ballistic Effects

Normal accelerations into propellant.- Test motors were fired at various pressure levels from 300 to 850 psia (2.07 to 5.85 MN/m^2) and at 0g, 40g, 60g, 80g, 100g, 120g, 200g, and 300g normal acceleration levels into the propellant surface. The variation of the burning rate with pressure for the nine normal acceleration levels is shown in the log-log plots of figure 10. The burning-rate data obtained from each normal acceleration test are presented and a least-squares fit of the data to Vieille's burning-rate equation $r = a\left(\frac{p}{500}\right)^n$ (ref. 7) is shown. The values of the burning rate constant a, and the exponent n, as calculated from the least-squares fit, are also indicated for each acceleration level. Both the burning-rate constant a and the pressure exponent n were found to be a function of the normal acceleration level. The constant a increased from 0.293 in./sec to 0.363 in./sec as the acceleration was increased from 0g to 300g. The pressure exponent increased from 0.326 to a maximum of 0.438 at 80g.

Figure 11 is a composite burning-rate pressure curve for normal accelerations of 0g, 40g, 60g, 80g, 100g, 250g, and 300g. The figure indicated the continual increase in average burning rate as the normal acceleration level was increased from static conditions to 300g. (The data from the 120g and 200g tests have been omitted for clarity.)

A cross plot of the least-squares burning-rate data as a function of normal acceleration at various pressure levels is presented in figure 12. This figure indicates that at a given operating pressure, the propellant possessed two distinct regions of sensitivity of the burning rate to normal accelerations. The propellant was most sensitive to increased normal accelerations in the acceleration region below 120g. As the acceleration level was increased above 120g, the burning-rate sensitivity underwent a transition and tended to increase at a greatly reduced rate at the higher acceleration levels. The decreased sensitivity in the higher acceleration region indicates a saturation of the mechanism causing the burning-rate increase.

The lines of constant-percent increase in burning rate, shown in figure 12, indicate the pressure dependence of the effects of normal acceleration on propellant burning rate. At a pressure of 300 psia (2.07 MN/m^2), a normal acceleration of 234g was required to produce a 20-percent increase in burning rate. However, a 20-percent increase in burning rate occurred at a normal acceleration level of 82g at an average chamber pressure of 1000 psia (6.89 MN/m^2).

The burning-rate curve at 500 psia (3.447 MN/m^2) in figure 12 also indicates the variation in the rate constant a in the burning-rate equation $r = a\left(\frac{p}{500}\right)^n$ as a function of normal acceleration.

The variation in the pressure exponent n as a function of normal acceleration is shown in figure 13. For acceleration levels as high as 80g, the pressure exponent increased linearly with increasing normal acceleration. At accelerations greater than 80g, the pressure exponent decayed exponentially with acceleration to a constant value of 0.40 at 200g. For accelerations greater than 200g, considerable scatter occurred in the exponent data and the constant value of 0.40 was assumed in this region for the purpose of generating a burning-rate equation. This scatter in the exponent data was probably due to the limited number of tests that were made at each acceleration level coupled with the increased variation in the burning-rate data at the higher acceleration levels.

The burning-rate equation $r = a\left(\frac{p}{500}\right)^n$ was modified to include the effects of normal acceleration by replacing the constant a, and the exponent n, by their respective function of normal acceleration as derived from figures 12 and 13. The empirical equation

$$r_g = \left[0.293 + 4.848 \times 10^{-6}(a_n^2)\right] \left(\frac{p}{500}\right)^{(0.326+1.4\times10^{-3}a_n)}$$

was found to describe the average burning rate as a function of normal acceleration in the acceleration region between 0g and 80g and for chamber pressures between 300 and 1000 psia. Comparison of this equation with the results of the burning-rate equations generated from the least-squares fit of the rate data indicates that this empirical equation predicts the burning rate rather well within the specified range of parameters. The maximum deviation $\left(\frac{r_g}{r - 1}\right) \times 100$ from the fitted data shown in figure 10 was less than 1 percent.

In like manner the empirical equation

$$r_g = 0.324 + 6.86 \times 10^{-3}\left(a_n - 80\right)^{1/3} \left(\frac{p}{500}\right)^{0.400} \exp\left[3.18238 \times 10^{-25}\left(300 - a_n\right)^{10}\right]$$

was found to represent the average burning rate as a function of normal acceleration in the acceleration region between 80g and 300g and for pressures between 300 and 1000 psia. The maximum deviation $\left(\frac{r_g}{r - 1}\right) \times 100$ from the fitted data shown in figure 10 was less than 1 percent for accelerations less than 120g and was slightly over 2 percent for accelerations greater than 120g.

Note, that since these equations are empirical equations derived with the U.S. Customary Unit System, it is necessary that pressure be given in pounds per square inch absolute, acceleration in g, and burning rate in inches per second. The burning-rate equations presented herein are for the average burning rate of a 1/2-inch-thick (12.7 mm) propellant slab. Since the pressure histories from these tests and the results from the

extinction tests indicated transient combustion phenomena present under the acceleration conditions, caution should be exercised in the use of these equations in predicting ballistic performance of other rocket motors with different propellant thicknesses.

Inclined accelerations.- From the results of the normal acceleration tests, it was initially postulated that as the orientation of the burning surface was varied, the burning rate would also vary as a function of the normal-acceleration component. The effects of orientation on burning-rate ratio at 200g centrifugal acceleration are presented in figure 14. The test results shown in this figure indicate that at orientations less than 75°, the resultant normal acceleration component had no appreciable effect on the propellant burning rate. These results indicate that the reduction in spin sensitivity, shown in figure 3 for the NOTS 551 motor, as a result of the longitudinal acceleration component may be explained by the shift in acceleration vector with respect to the propellant burning surface. The NOTS 551 data indicate only slight deviations from static motor performance until the spin rate and longitudinal acceleration were such that the resultant vector was at an angle of 65° into the propellant surface, at which time the motor spin rate was approximately 6 rps. During the ground spin test, a lower average spin rate resulted in the much increased pressure history shown in figure 3.

The orientation test results obtained in the test motor indicate that in the absence of spin-induced vortex-flow effects, motors with predominantly normal accelerations will be most severely affected by the imposed acceleration environment.

Also, normal acceleration away from the burning surface as high as 300g indicated no appreciable effect on burning rate. Further experiments are necessary to determine the effects in the undefined region at orientations between 75° and 90°.

Residue Effects

Postfire inspection of the lower inserts from motors fired with acceleration loads normal and into the propellant surface indicated the retention of metallic-like residue on the surface to which the propellant had been bonded. Representative photographs of the lower inserts from tests at static conditions and at normal acceleration levels of 80g, 200g, and 300g are shown in figure 15. No residue remained on the lower inserts of the motor fired under static conditions. In general, as the normal acceleration increased, the size and the amount of residue remaining increased. In the photographs for the 200g and 300g accelerations, notice the hollow appearance of the residue particles. Also, at the higher acceleration levels, the residue appears to have run together to form larger agglomerates. Since some data scatter in the size and the weight of the residue from individual motor firings at the same acceleration level was evident, average values of residue size and weight at each test condition are used in the discussion.

The results of the average residue size distribution data obtained at each acceleration level are shown in figure 16. On the figure are listed the average weights retained on the lower inserts, average diameters, and the number of sieve analyses that were made of each acceleration level. The collection of the residue and the performance of a sieve analysis with such small quantities of residue resulted in considerable data scatter. Occasionally, some of the residue was inadvertently lost during motor disassembly. Figure 16 indicates that although the average size of the residue – the size at the 50-percent retention point – varied from 0.028 to 0.065 inch (0.711 to 1.651 mm), the distributions of the residue diameters were essentially unchanged by the increased normal acceleration. (The odd shape of the distribution curve at the 60g level was thought to be due to errors caused by small sample size.)

Figure 17 shows the variation of the average residue diameter and average residue weight retained on the lower inserts as a function of the normal acceleration level. Although some scatter occurred, the figure indicates the increase in average residue particle size and average residue weight as the normal acceleration was increased from static to 300g. The average residue particle diameter increased to 0.065 inch (1.651 mm) at a normal acceleration level of 300g. The average weight of the residue retained at this acceleration level was 3.5 grams. This 3.5 grams was approximately 1 percent of the propellant slab weight.

There was no apparent correlation between residue weight and chamber pressure (correlation might have been masked by residue-weight data scatter); therefore, the burning-rate ratio at 500 psia (3.45 MN/m^2) was used to determine any correlation between residue weight and propellant burning rate. Figure 18 relates the increase in average metallic residue weight at motor burnout with burning-rate ratio. In all cases, increased burning rate was associated with increased residue weight.

The increase in energy release by burning metal retained on the propellant surface has been proposed in a theoretical model to explain the increase in average burning rate under acceleration conditions. (See refs. 5 and 6.) The change in sensitivity of the burning-rate ratio with increasing average residue weight shown in figure 18 is an indicator of the complexity of the role that the residue plays in burning-rate augmentation. Such effects as the changes in residue chemical content, residue size, residue number density, and the time dependency of these parameters with acceleration loads should also be considered in any theoretical modeling of the combustion process. Chemical analyses of two residue samples indicated that the metallic aluminum in the residue increased from approximately 3.4 percent at 80g to 6.4 percent at 300g normal acceleration. Inspection of the lower inserts from motors fired at orientations other than normal and into the burning surface indicated that no residue remained on the lower inserts of motors fired under these conditions.

Extinction Tests

In order to gain a better understanding of the observed combustion phenomena, the test motor was modified to allow examination of the extinguished propellant surface after burning for various times at various acceleration levels and orientations. Several tests were conducted under static conditions to demonstrate the technique and determine the condition of the propellant surface after rapid depressurization and water quench. Figure 19(a) is a photograph of the propellant surface following a static extinction test at 0.5-second burning time. The propellant surface was smooth, and there were no indications of uneven ignition of the propellant surface or irregularities resulting from the extinction process. (The two small ridges at the ignitor end of the grain were probably caused by inhibitor failure at the edge.)

Figures 19(b) and 19(c) are photographs of the propellant surface after tests at 100g normal acceleration into propellant for 0.5 second and 1.5 seconds, respectively. Figure 19(b) shows that after the 0.5-second burning time, a number of small pits have begun to form on the propellant surface. (The varying tone of the propellant surface is caused by water standing on grain after firing.) Figure 19(c) shows a considerable increase in the size of the pits as the burning time was increased to 1.5 seconds. This increasing pit size as a function of time at constant acceleration level indicated the transient nature of the combustion process. The localized increased burning rate and the associated increased surface area under the acceleration environment was apparently a cause of the progressive pressure histories observed and the increased average burning rate. Figure 19(c) also shows some of the metallic residue remaining in the pits on the propellant surface even after the violent extinction process.

Figure 19(d) is a photograph of the propellant surface following a test at 40g normal acceleration for 1.5 seconds. Comparison of figures 19(c) and 19(d) indicates the effect of acceleration level on the number of pits and the pit size for the same burning time. As the acceleration level was increased, both the size and the number of pits on the propellant surface increased for a given burning time. The larger pit in the upper quadrant was thought to be caused by a void in the propellant.

Figure 19(e) is a photograph of the propellant surface obtained after 1.5-second burning time at 100g and at the 60^{o} orientation. Most of the propellant surface remained very smooth and was similar to that for the static test. However, a row of pits occurred adjacent to the motor wall on the outward side of the motor away from the centrifuge axis. The presence of pitting along this outer edge indicates that under inclined acceleration loads, the condensed phase combustibles are forced to migrate across the propellant surface and thus cause increased localized burning only where it is retained by the motor wall. This limited pitting indicated that only a fraction of the condensed phase in

the propellant is associated with localized burning-rate augmentation in tests at inclined orientations. It could not be determined from these tests whether the inclined orientations prevented the formation of metallic agglomerates on the surface or whether the migration across the surface enhanced agglomerate combustion and thus reduced the amount of residue at extinction.

The extinction tests were conducted with the use of a 0.40-inch-diameter (10.16 mm) nozzle throat which corresponds to a nominal static test pressure of approximately 350 psia (2.41 MN/m^2).

CONCLUDING REMARKS

At an average pressure of 500 psia (3.45 MN/m^2) and with the acceleration vector perpendicular and into the propellant burning surface, increasing the acceleration from 0g to 300g resulted in a 21-percent increase in average burning rate. When the chamber pressure was increased to 1000 psia (6.90 MN/m^2), the burning rate increased 33 percent when the acceleration level increased from 0g to 300g. Thus, the effect of acceleration on the burning rate was also found to be a function of the average chamber pressure.

Both the burning-rate constant a and the pressure exponent n in the burning rate equation $r = ap^n$ were found to be functions of the normal acceleration level. (The average burning rate during combustion of a 1/2-inch web was used in all burning-rate calculations.)

Burning-rate equations were generated to describe the burning rate of the polybutadiene acrylic acid propellant tested as a function of normal acceleration for pressures between 300 and 1000 psia (2.07 and 6.9 MN/m^2) and for acceleration levels to 300g. The propellant burning rate was most sensitive to increasing acceleration for acceleration levels less than 120g. When the acceleration vector was inclined at 75° or less with respect to the burning surface, the average burning rate was not significantly affected by acceleration levels as high as 300g centrifugal acceleration.

In the normal acceleration tests both the size and weight of the metallic residue remaining at motor burnout increased with increased normal acceleration. During the inclined orientation tests no significant residue remained on the lower inserts of the burned-out motors.

The presence of metallic residue in the pits of the propellant surface following the extinction tests was evidence that the retention of residue on the propellant surface was one cause of burning-rate augmentation of this composite propellant under acceleration conditions.

The increased pit size as a function of time indicated the transient nature of the combustion process under the normal acceleration environment. This time dependency

of the combustion process requires that time, or distance burned, be included in any combustion model or ballistic program to describe aluminized composite propellant combustion under an acceleration environment.

The data from the orientation tests indicate that extreme caution should be exercised in the extrapolation of ground-spin-test results to flight performance. Since the burning rate of the propellant is sensitive to the orientation of the acceleration vector with respect to the burning surface, the longitudinal acceleration imposed by flight can result in marked differences between ground spin and flight test results. Motors tested in environments where vortex flow is the main cause of the performance change will probably not be sensitive to the shift in the acceleration vector due to flight environment.

Changes in propellant formulation which tend to reduce the agglomeration of the metallic fuel additive will be effective in reducing the effect of acceleration on the combustion of aluminized composite propellants.

Langley Research Center,
National Aeronautics and Space Administration,
Langley Station, Hampton, Va., July 25, 1968,
128-32-06-02-23.

REFERENCES

1. Manda, Leo J.: Compilation of Rocket Spin Data. Vol. II: Literature Survey. Rep. No. 3001-2 (NASA CR-66641), Electron. and Space Div., Emerson Elec. Co., [1968].

2. Swain, Robert L.; Lucy, Melvin H.; Foss, Peter H.: Rocket-Motor Spin-Test Apparatus Presented at Second Annual Meeting of ICRPC Working Group on Static Testing, Oct. 1964.

3. Lucy, Melvin H.: Spin Acceleration Effects on Some Full-Scale Solid Rockets. AIAA Sounding Rocket Vehicle Technology Specialist Conference, Feb.-Mar. 1967, pp. 301-312.

4. Lucy, Melvin H.; Swain, Robert L.; and Hudson, John L., Jr.: Variable Dynamic Force Vector Rocket Test Apparatus. Presented at Second Annual Meeting of the ICRPC Working Group on Static Testing, Oct. 1964.

5. Crowe, C. T.: Investigation of Particle Growth and Ballistic Effects on Solid Propellant Rockets. UTC 2128-FR (Contract No. NOw 65-0222-f), United Technol. Center, June 15, 1966.

6. Glick, Robert L.: An Analytical Study of the Effects of Radial Acceleration Upon the Combustion Mechanism of Solid Propellant. Rep. No. 42-66 (NASA CR 66218), Thiokol Chem. Corp., Dec. 1966.

7. Barrére, Marcel; Jaumotte, André; DeVeubeke, Baudouin Fraeijs; and Vandenkerckhove, Jean: Rocket Propulsion. Elsevier Pub. Co., 1960.

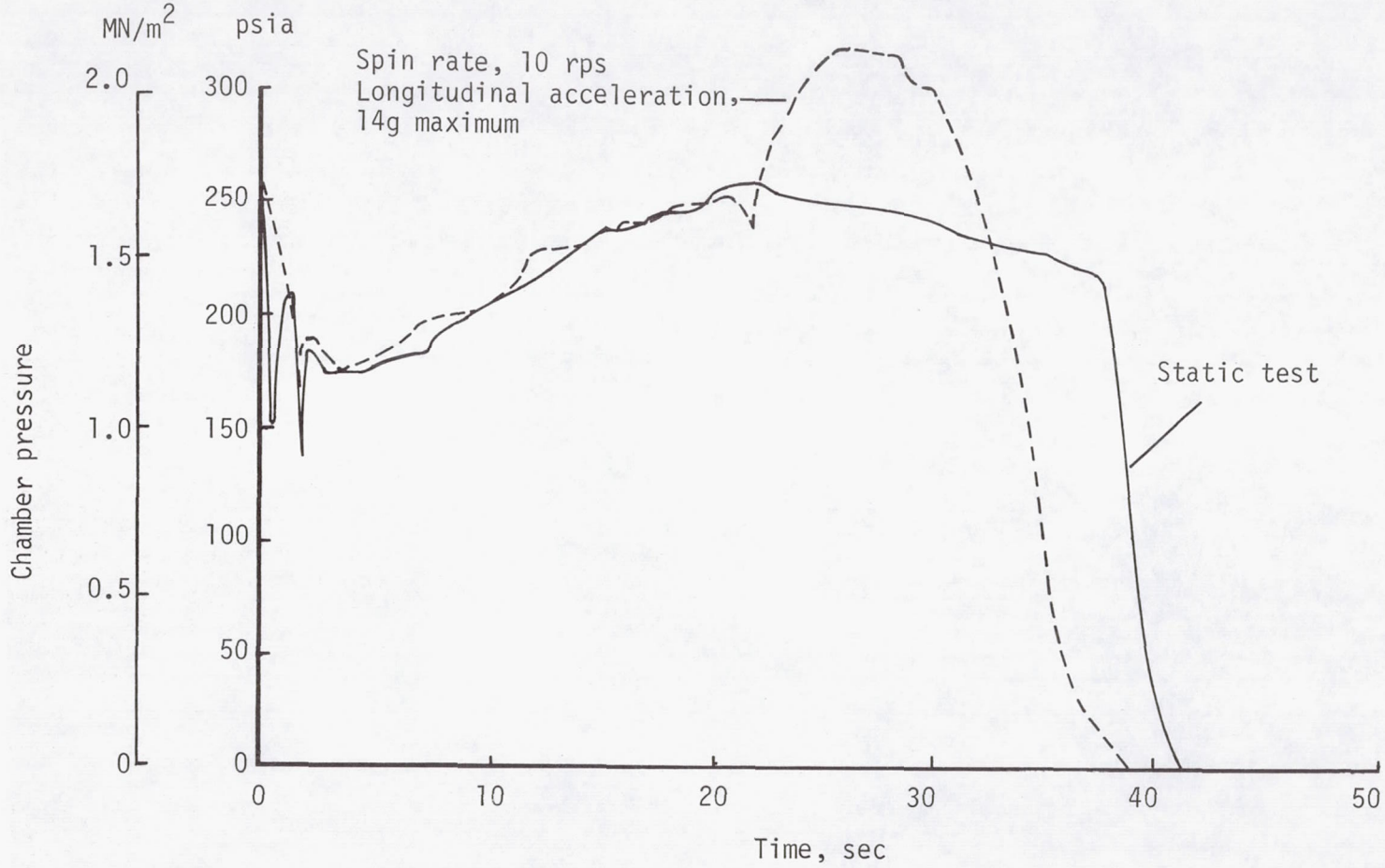

Figure 1.- Altair I flight and static-pressure time histories.

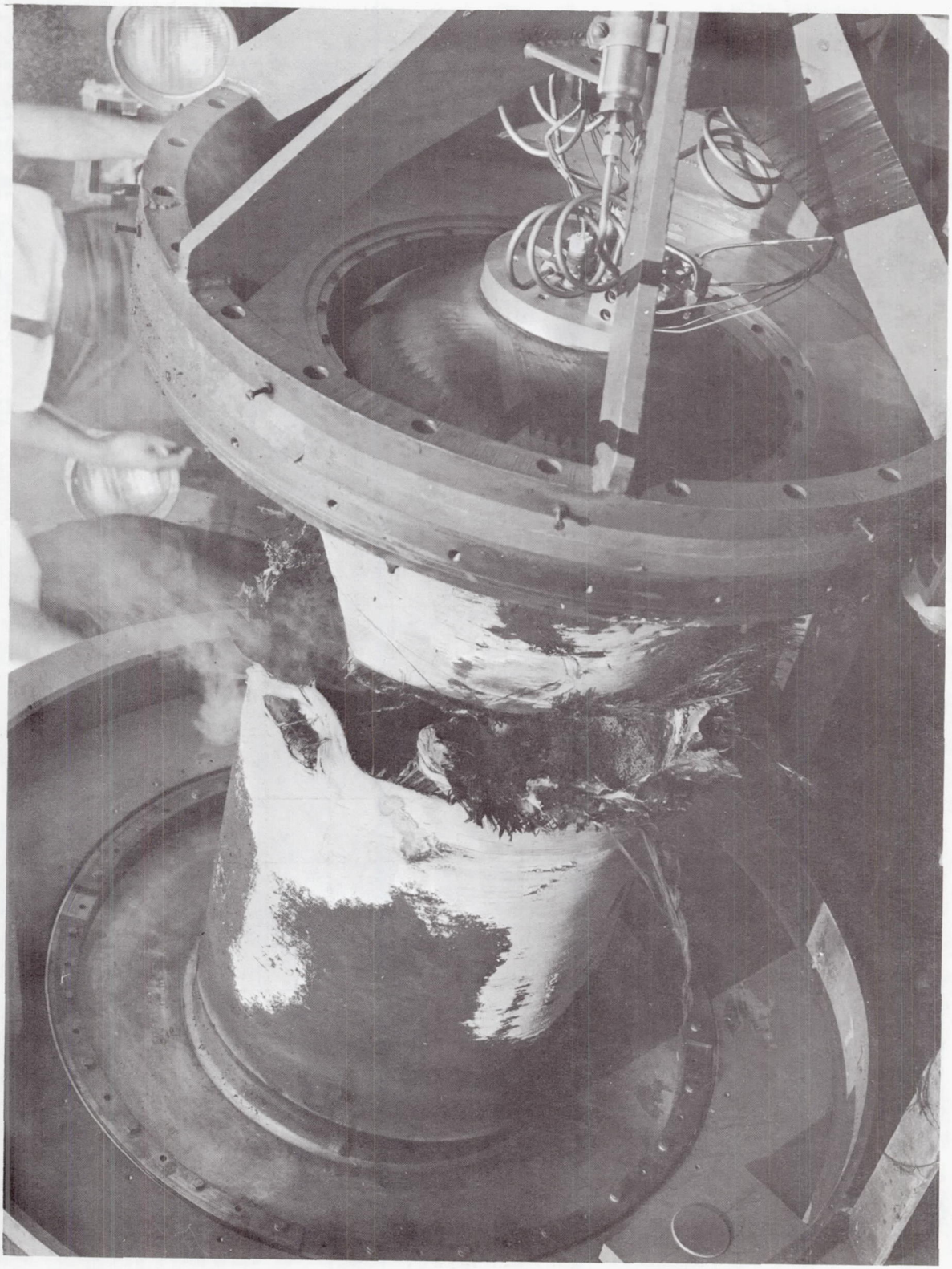

Figure 2.- Altair II postfire condition.

L-63-4547

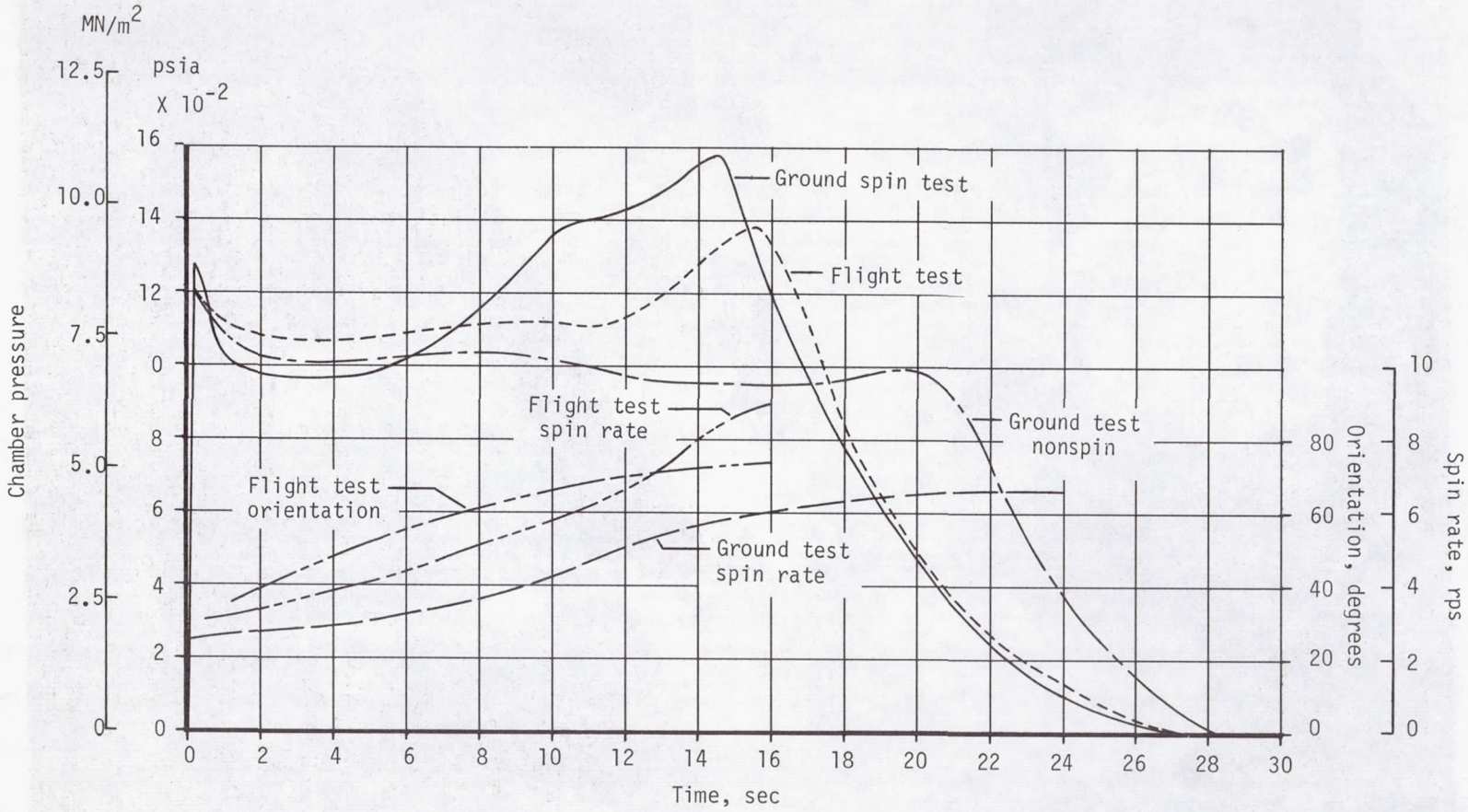

Figure 3.- NOTS 551 pressure time histories.

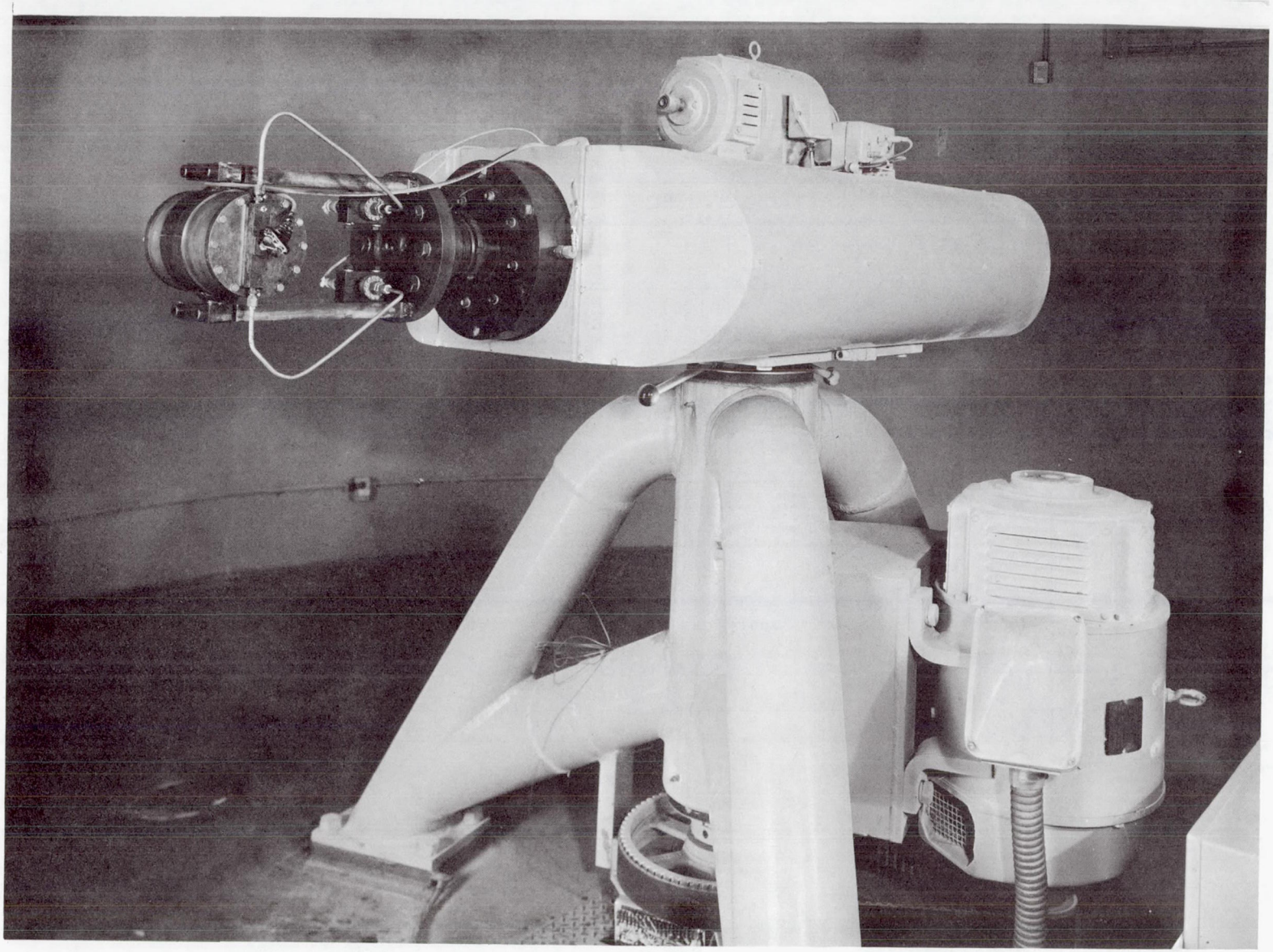

Figure 4.- Centrifuge. L-65-2915

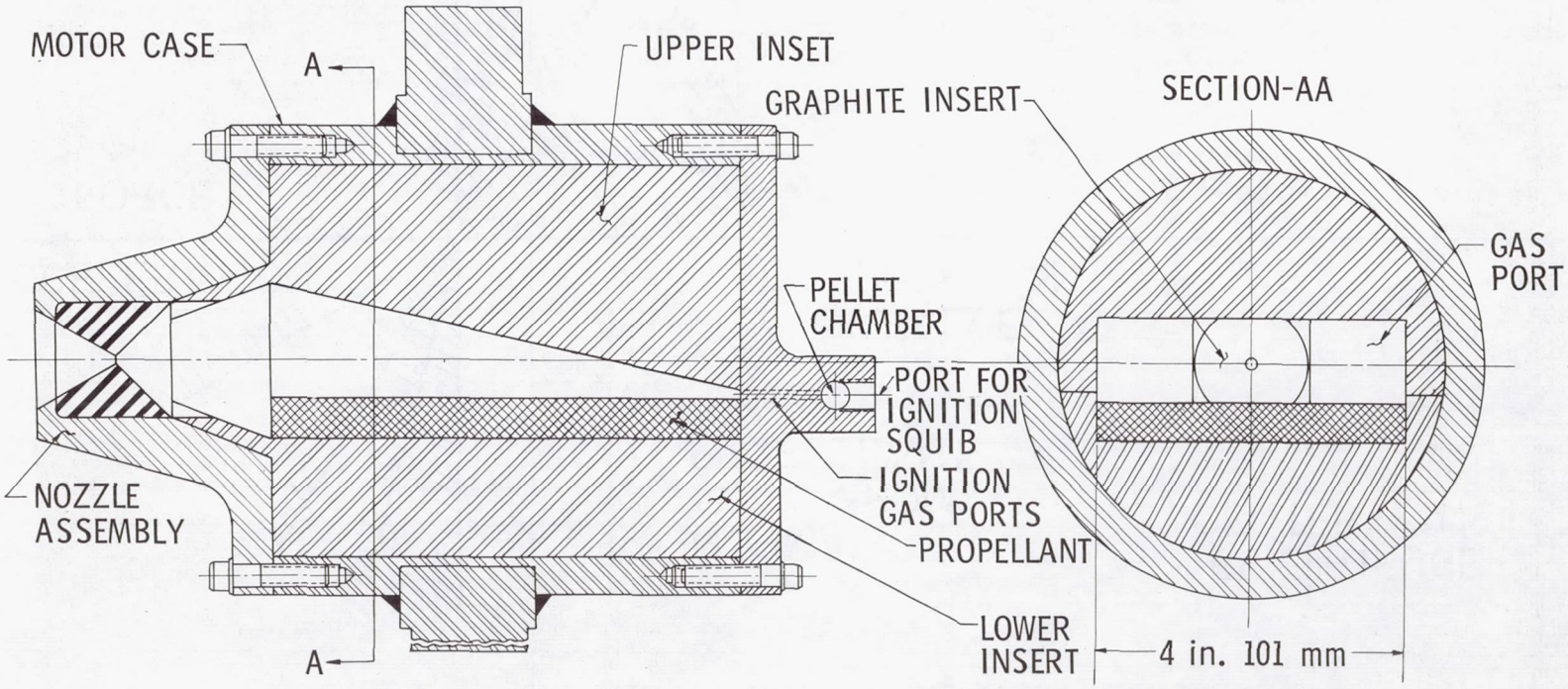

Figure 5.- Test motor cross section.

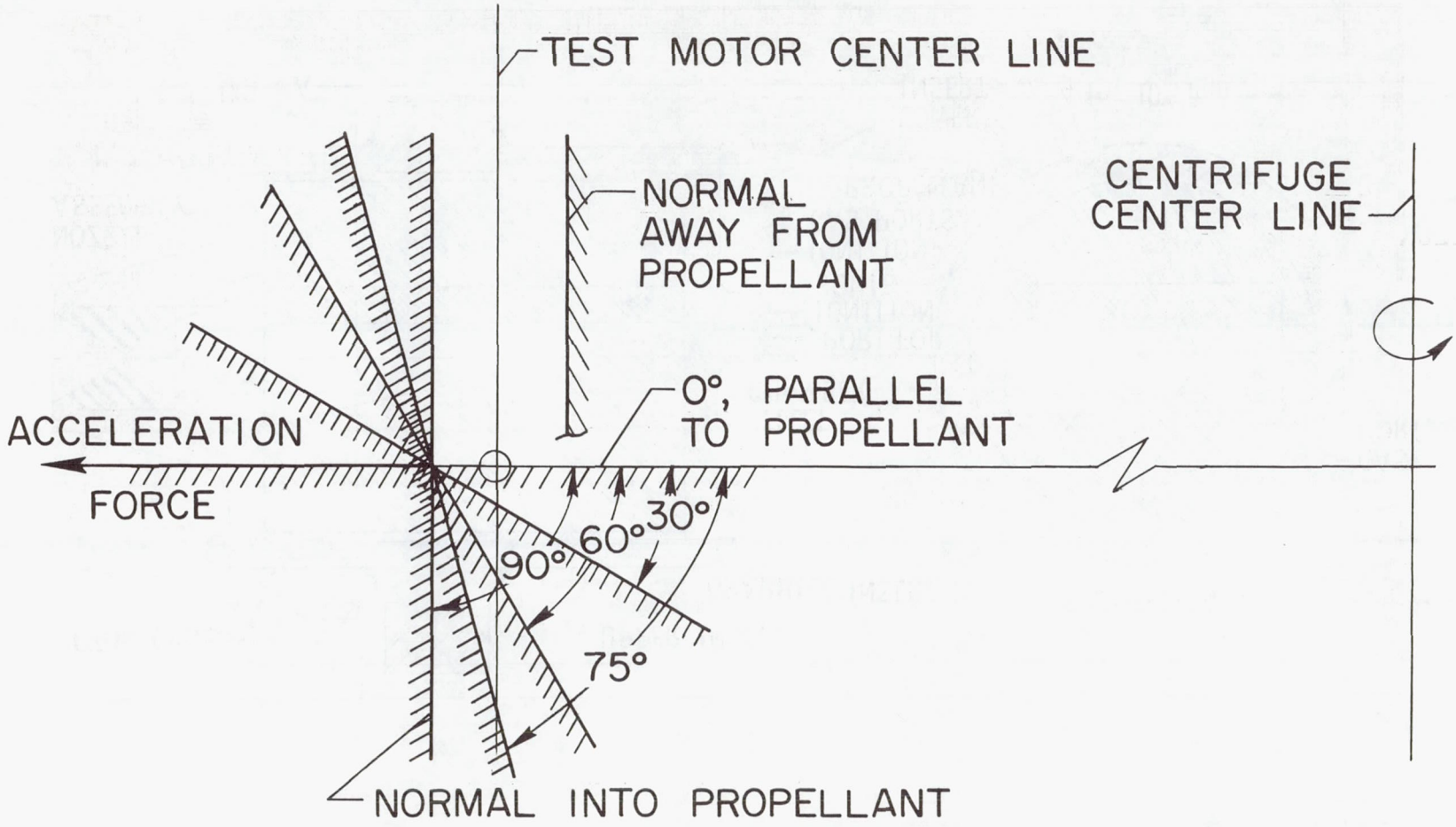

Figure 6.- Test orientations of propellant.

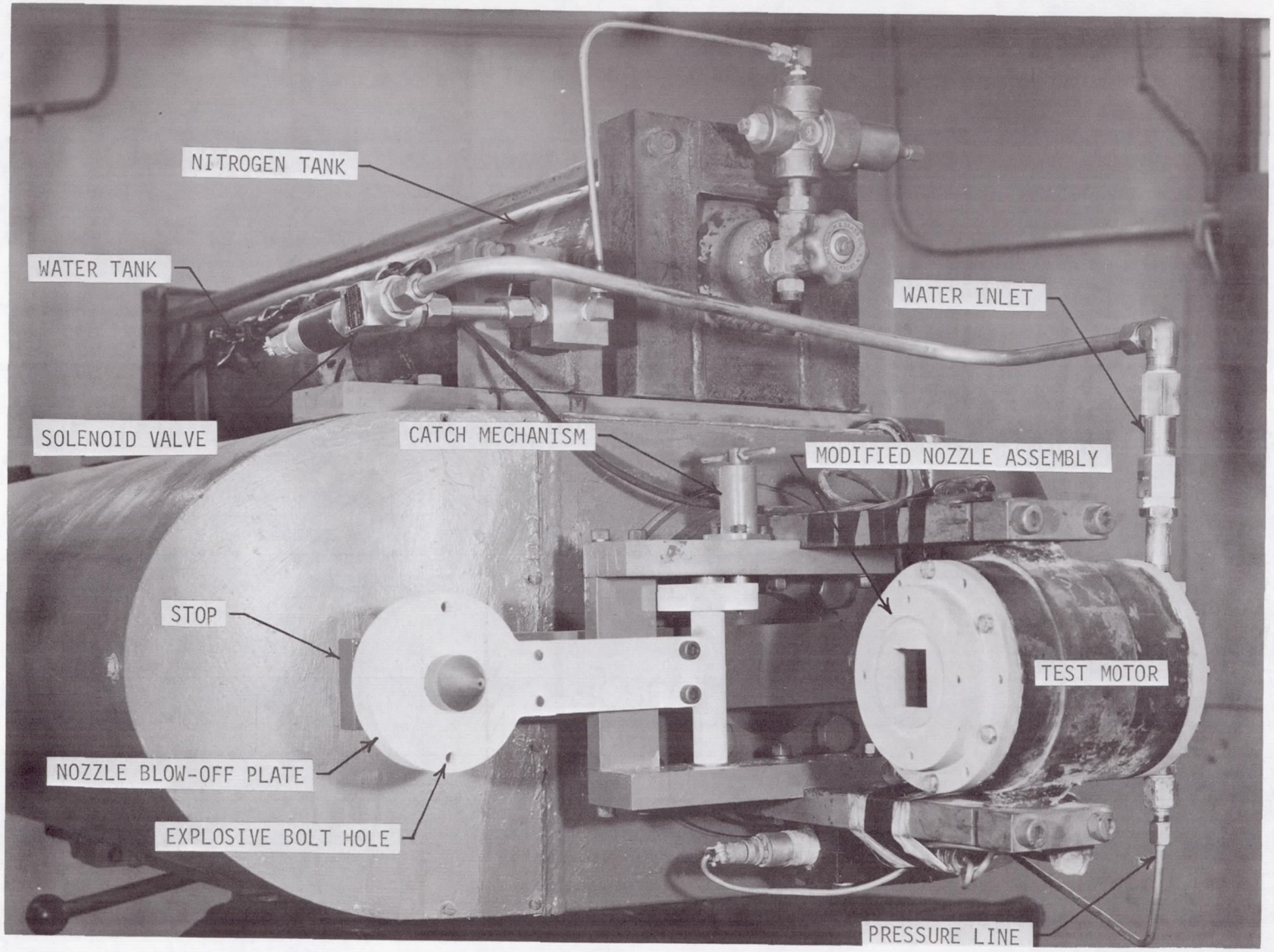

Figure 7.- Extinction test apparatus.

L-66-5813.1

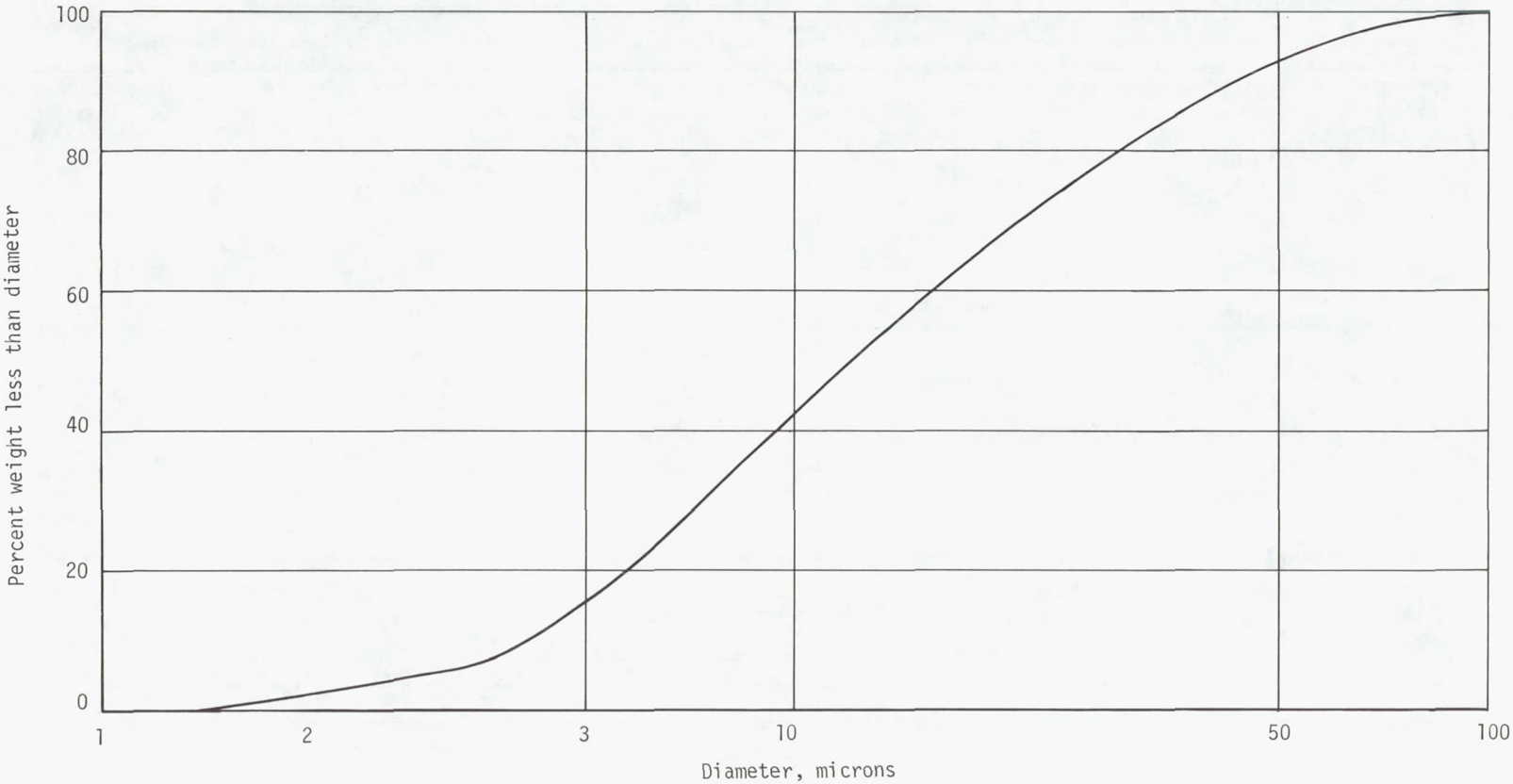

(a) Ground ammonium perchlorate.

Figure 8.- Particle size distribution.

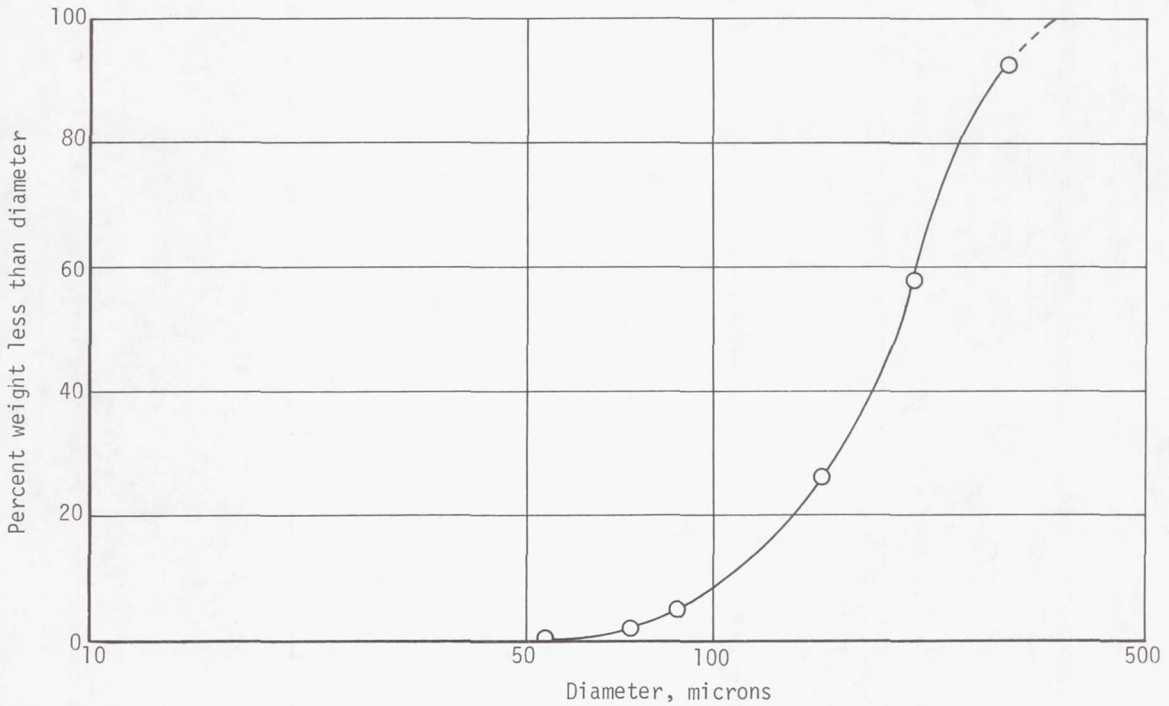

(b) Unground ammonium perchlorate.

Figure 8.- Continued.

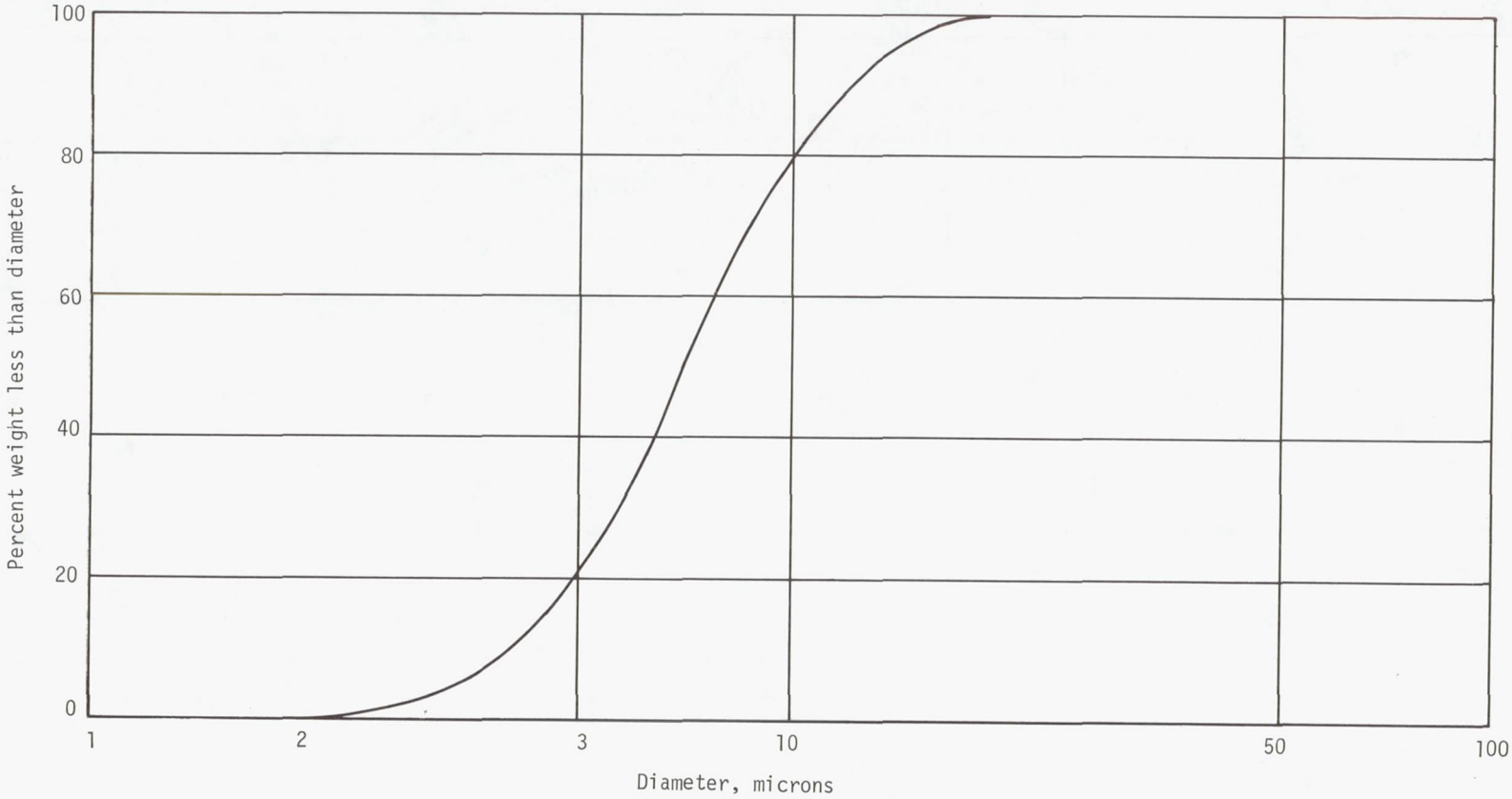

(c) Aluminum.

Figure 8.- Concluded.

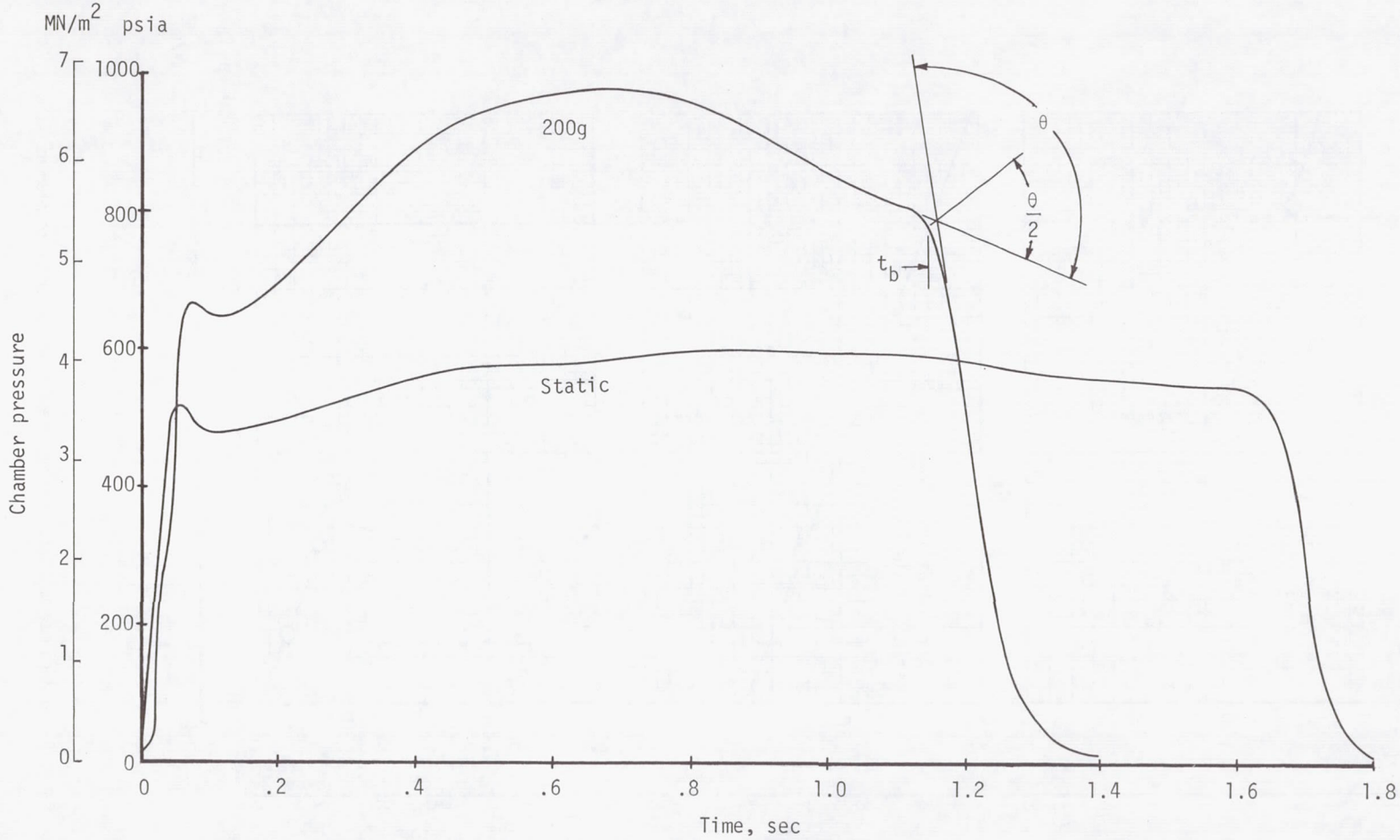

Figure 9.- Test motor pressure time histories.

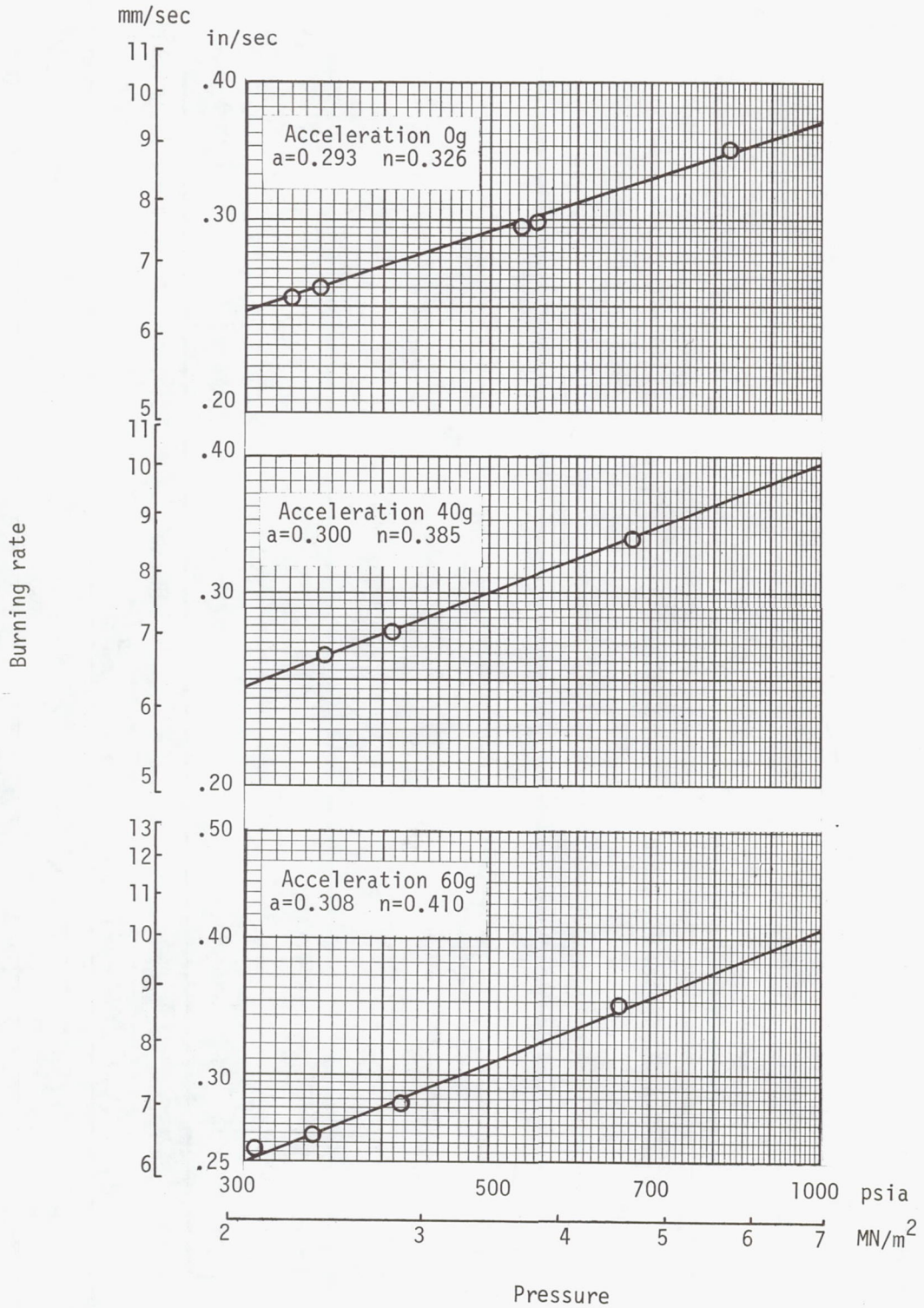

Figure 10.- Burning rate as a function of pressure for various normal accelerations.

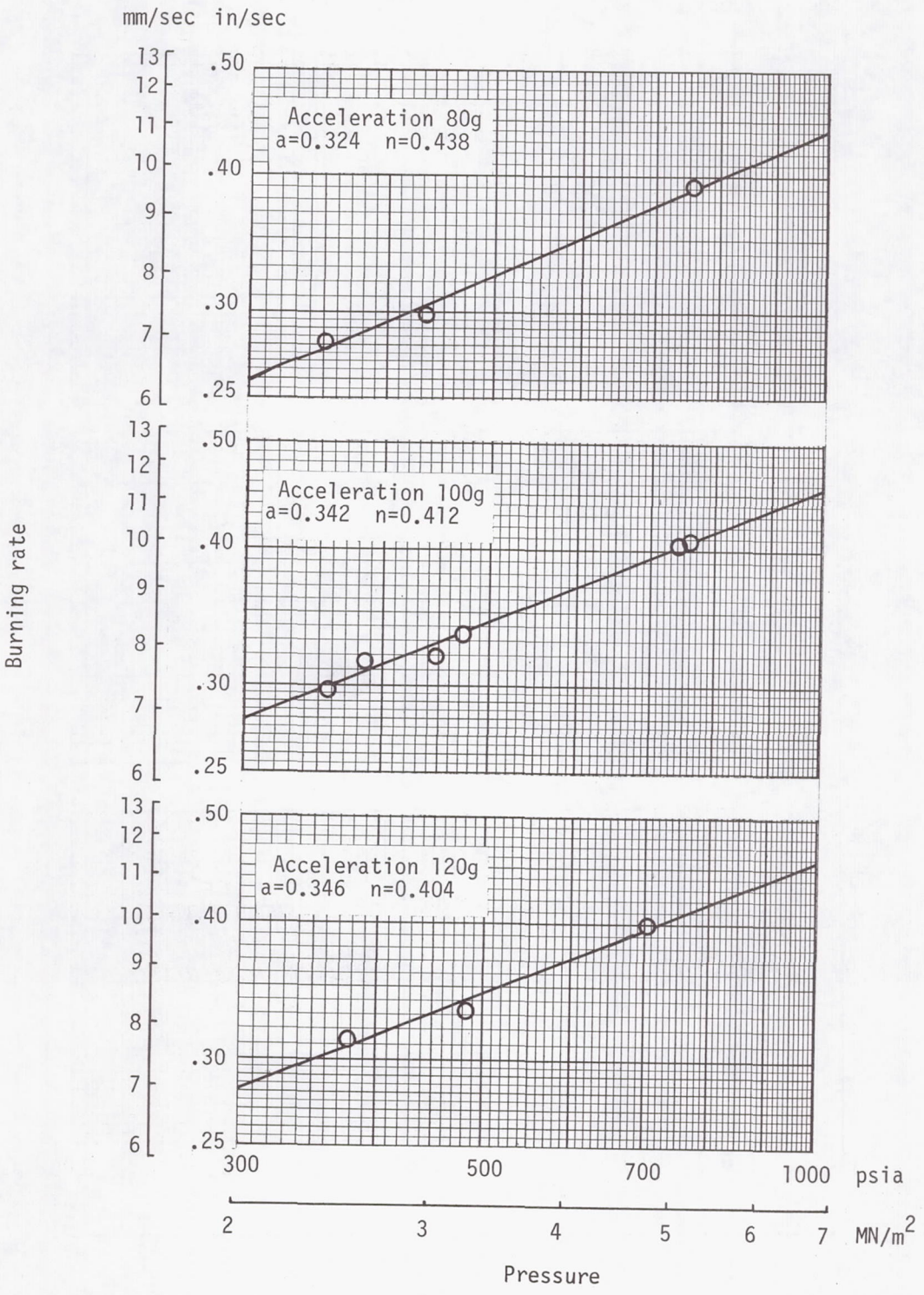

Figure 10.- Continued.

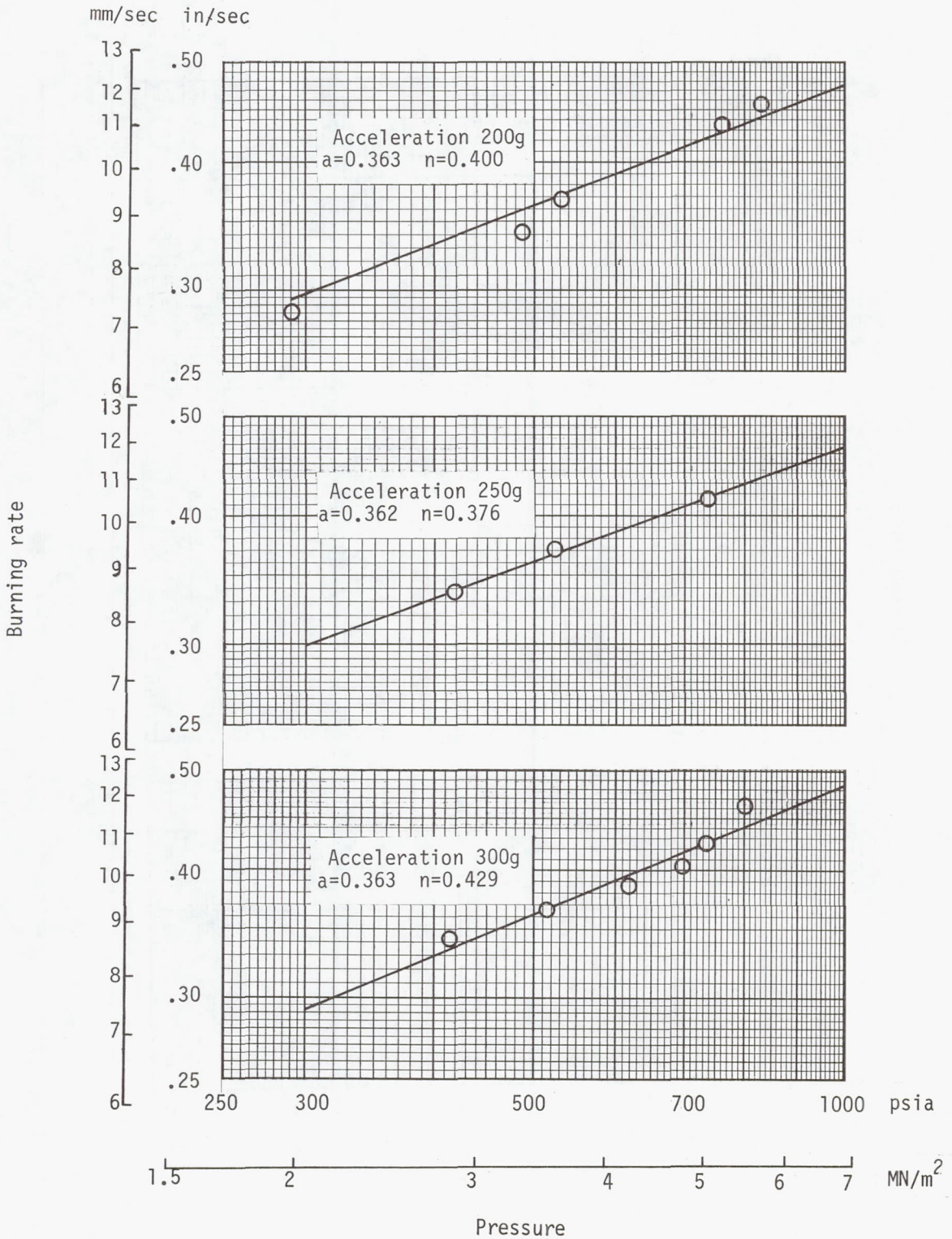

Figure 10.- Concluded.

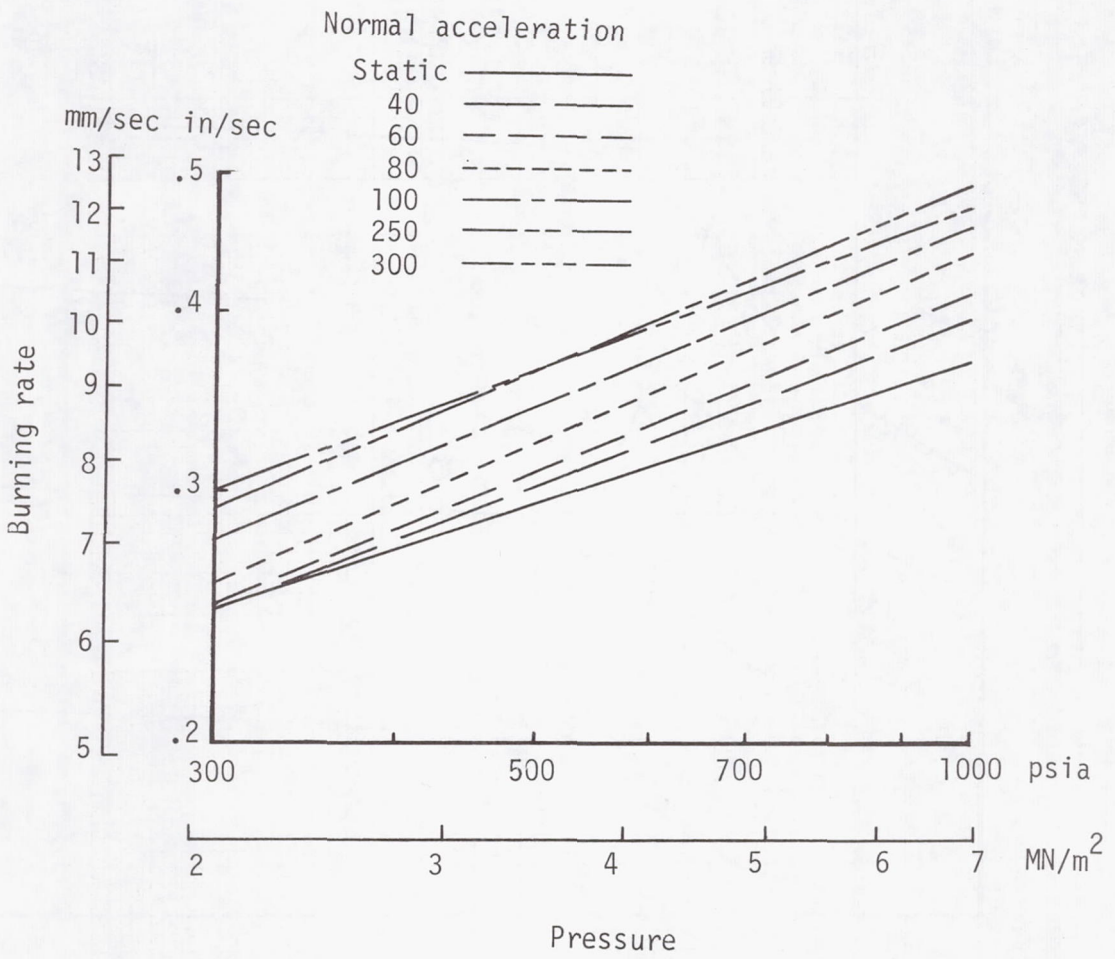

Figure 11.- Composite burning-rate curve.

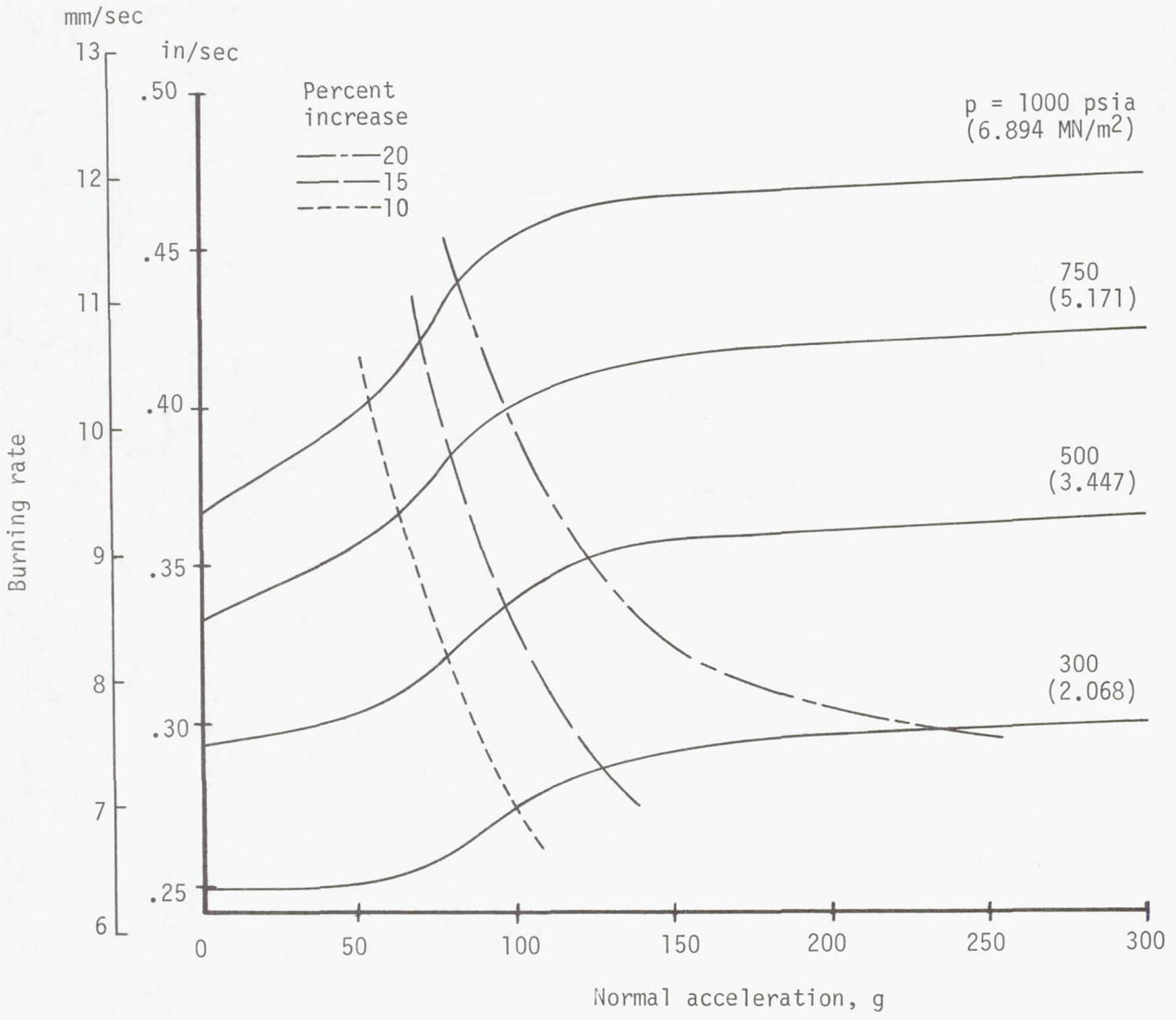

Figure 12.- Effects of normal acceleration on burning rate for various pressure levels.

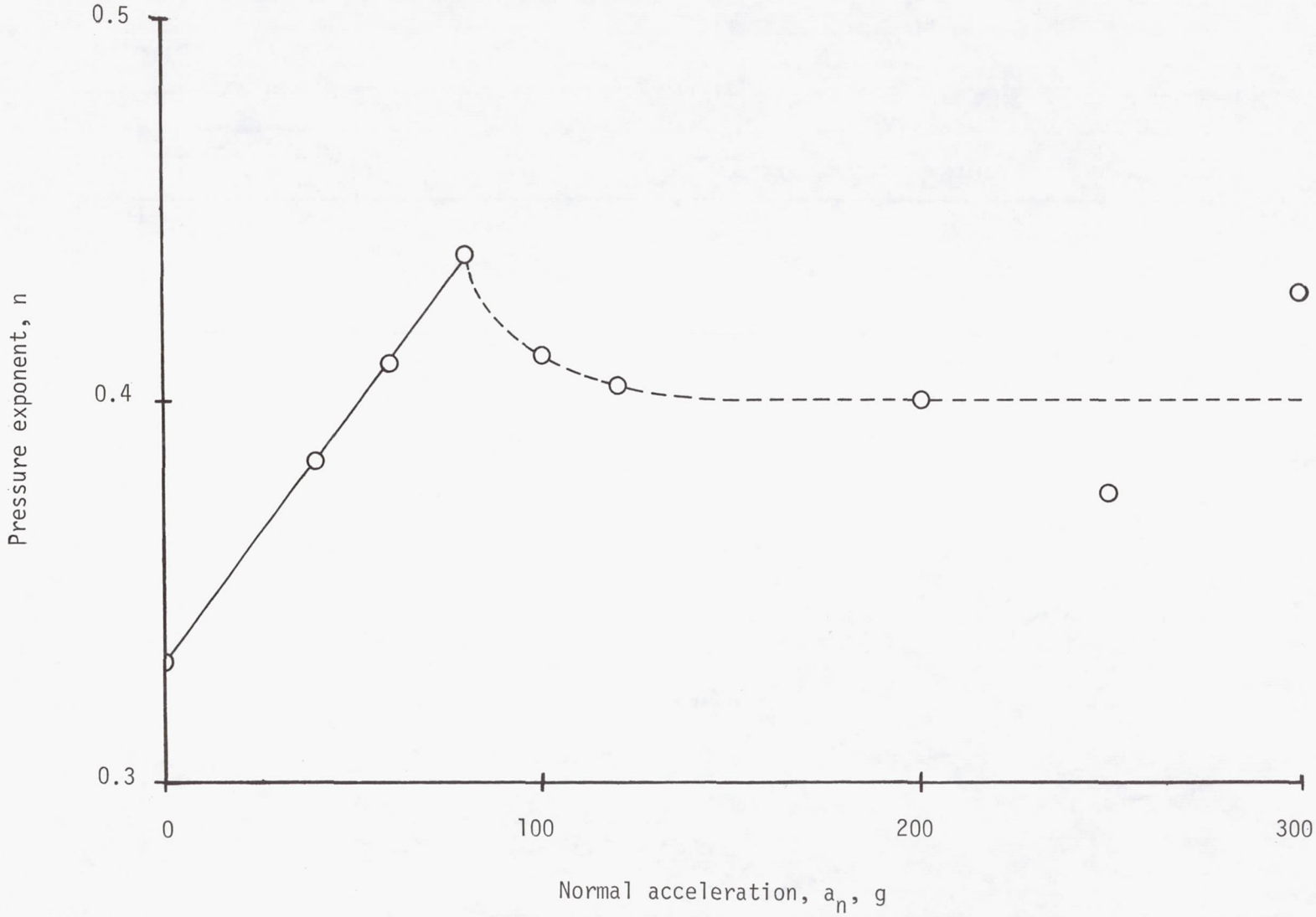

Figure 13.- Effect of normal acceleration on the pressure exponent.

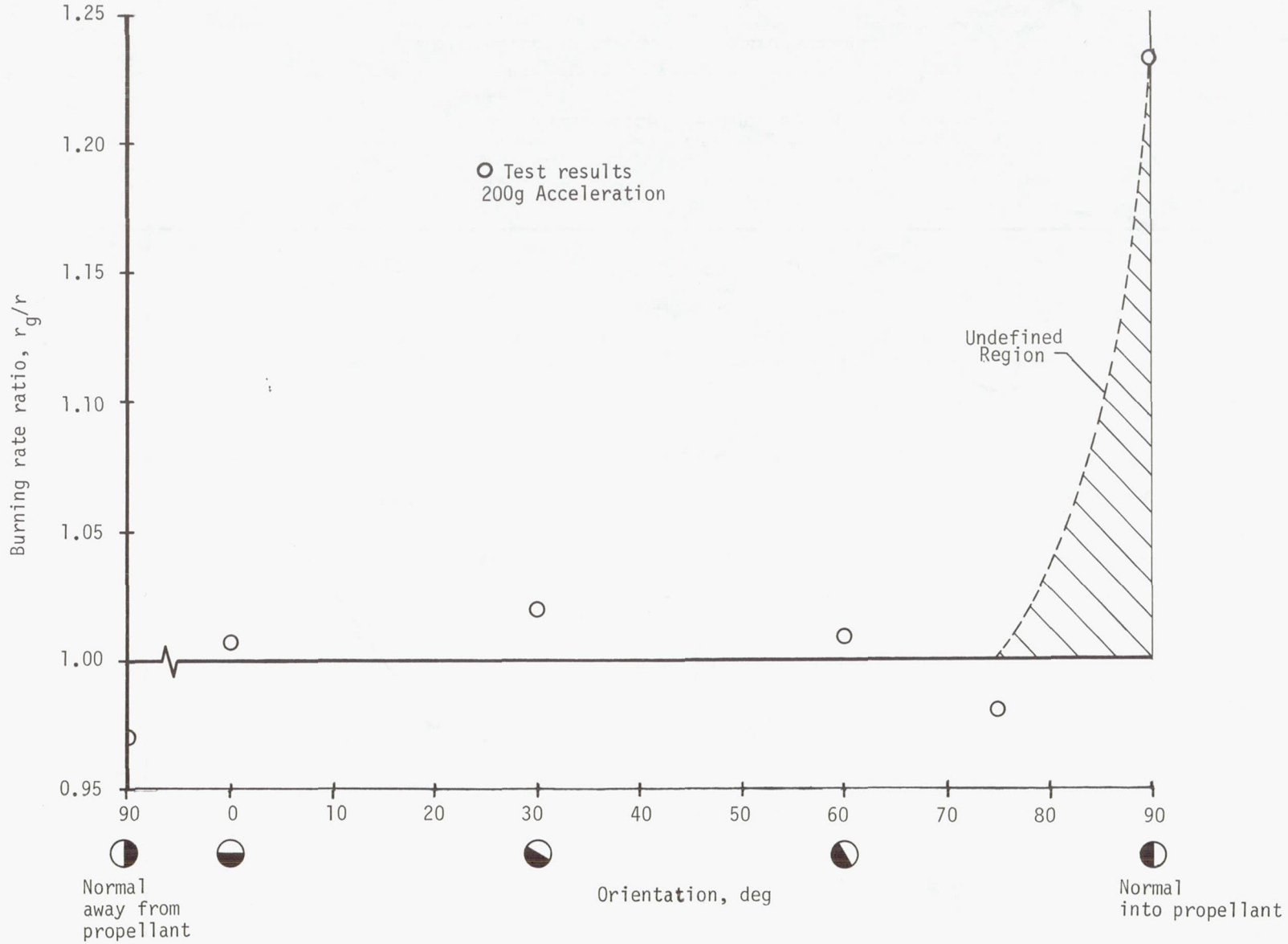

Figure 14.- Effect of propellant orientation on burning rate.

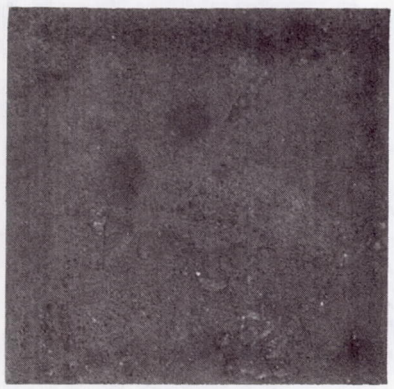

STATIC

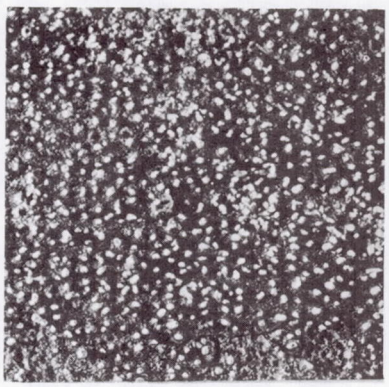

80 g

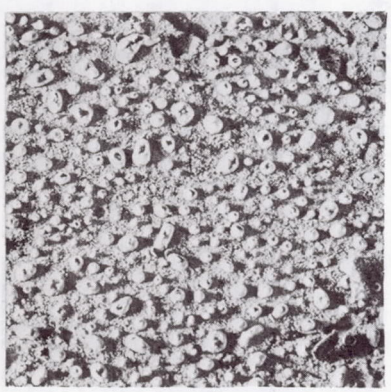

200 g

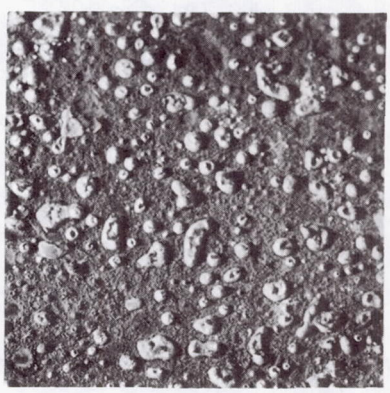

300 g

Figure 15.- Residue retained on lower insets after normal acceleration test. L-2699-10

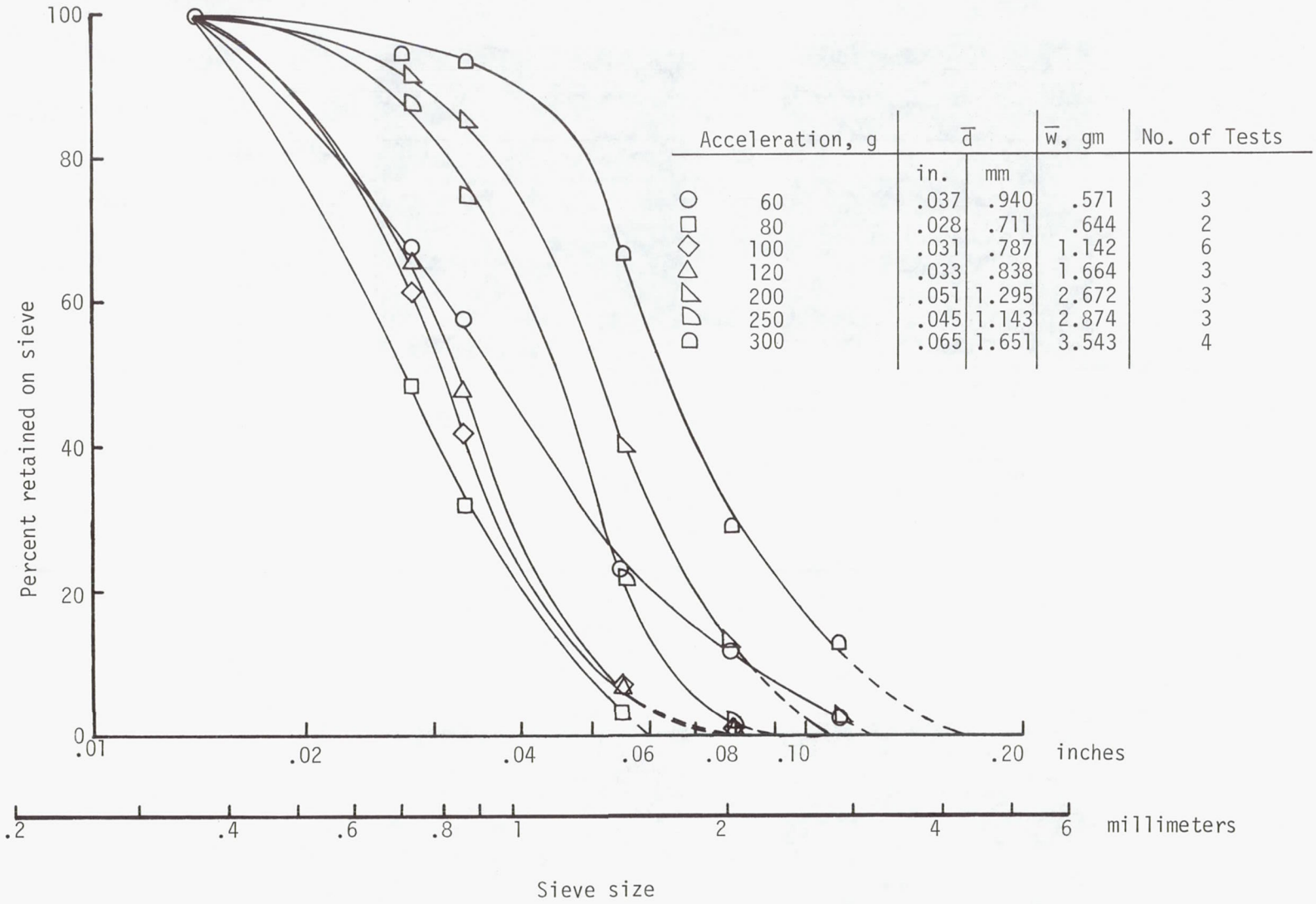

Acceleration, g	$\bar{d}$		$\bar{w}$, gm	No. of Tests
	in.	mm		
○ 60	.037	.940	.571	3
□ 80	.028	.711	.644	2
◇ 100	.031	.787	1.142	6
△ 120	.033	.838	1.664	3
◿ 200	.051	1.295	2.672	3
▱ 250	.045	1.143	2.874	3
▱ 300	.065	1.651	3.543	4

Figure 16.- Residue size distribution curves.

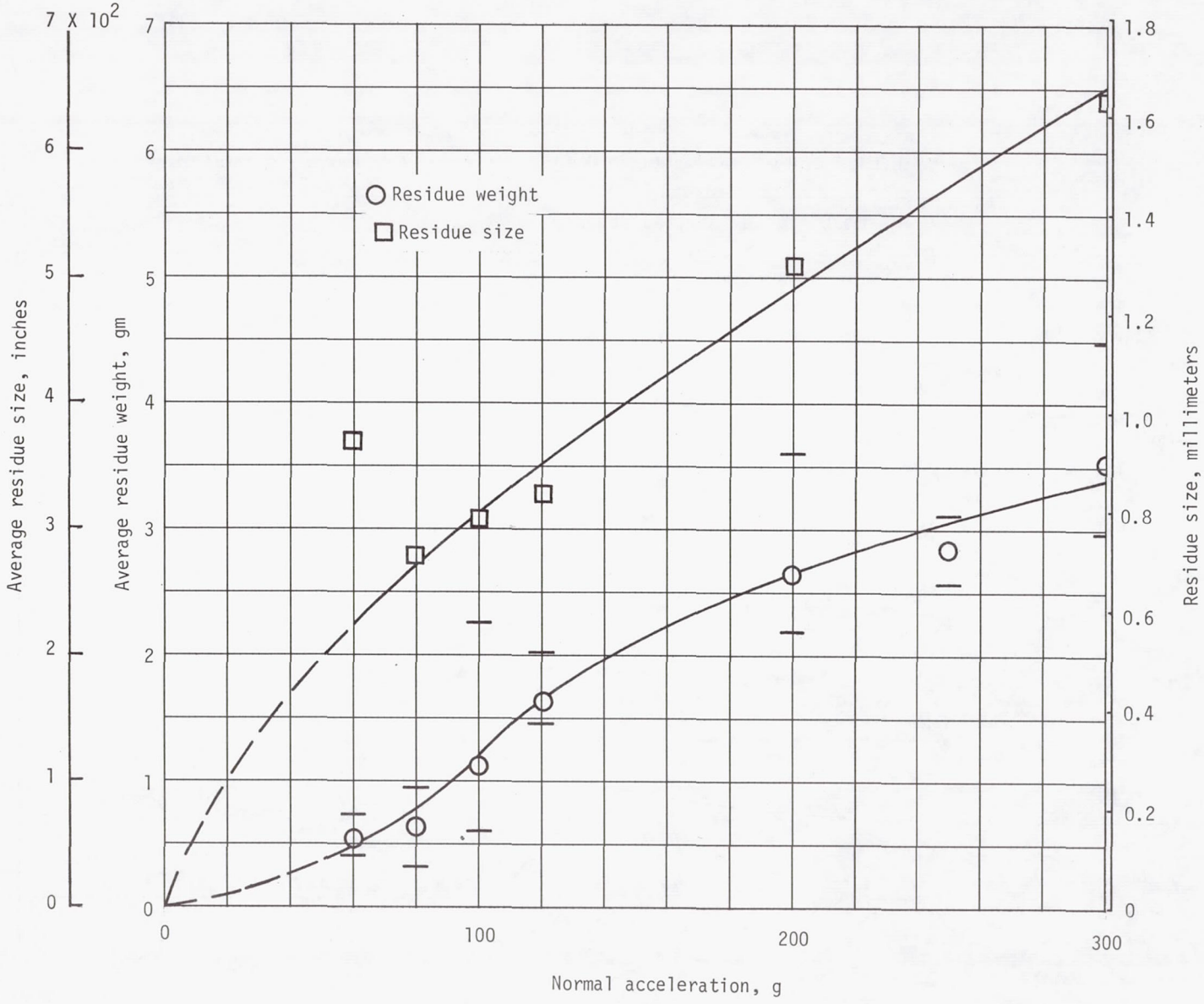

Figure 17.- Effect of normal acceleration on residue size and weight.

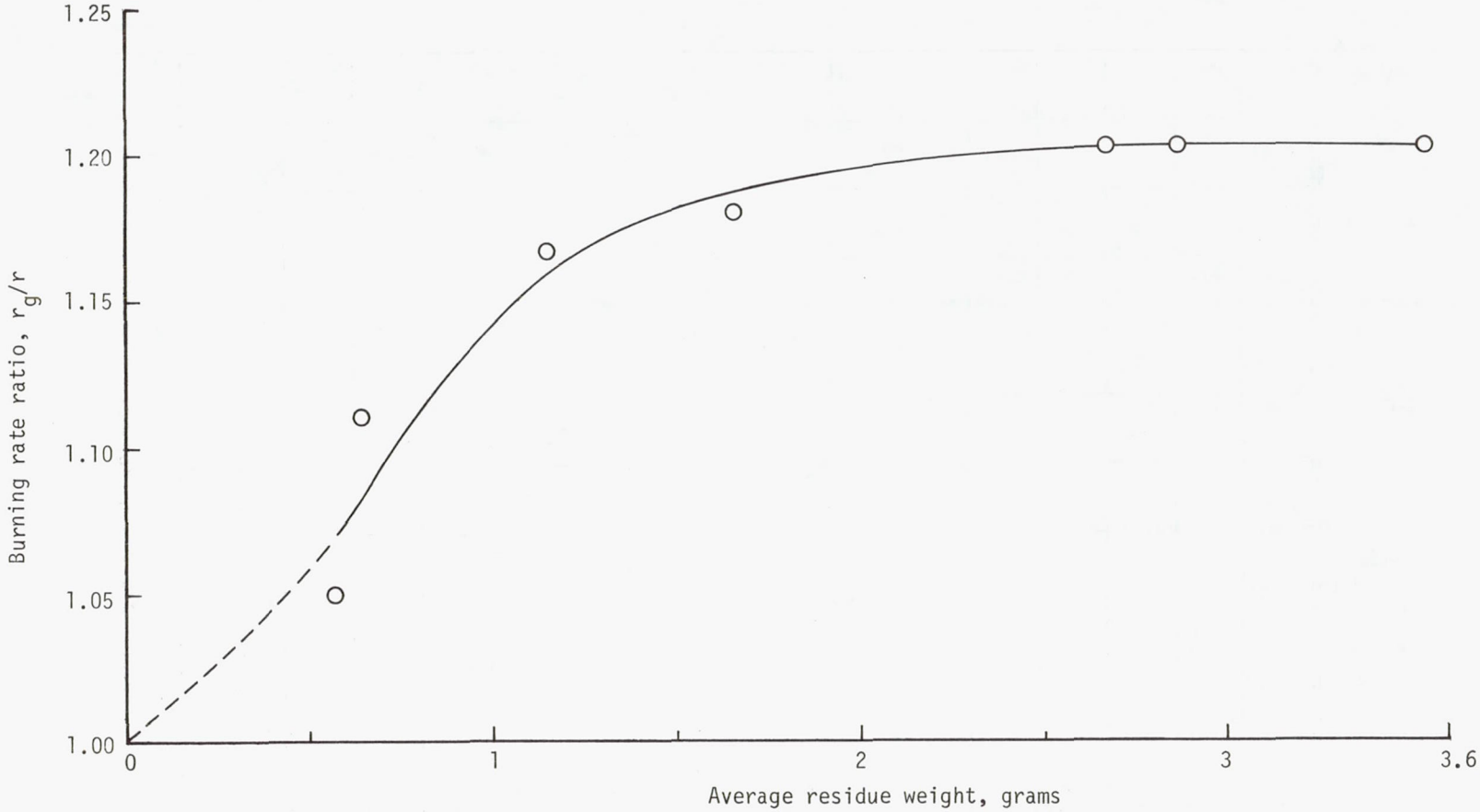

Figure 18.- Relationship of residue weight and propellant burning-rate ratio at 500 psia (3.45 MN/m^2).

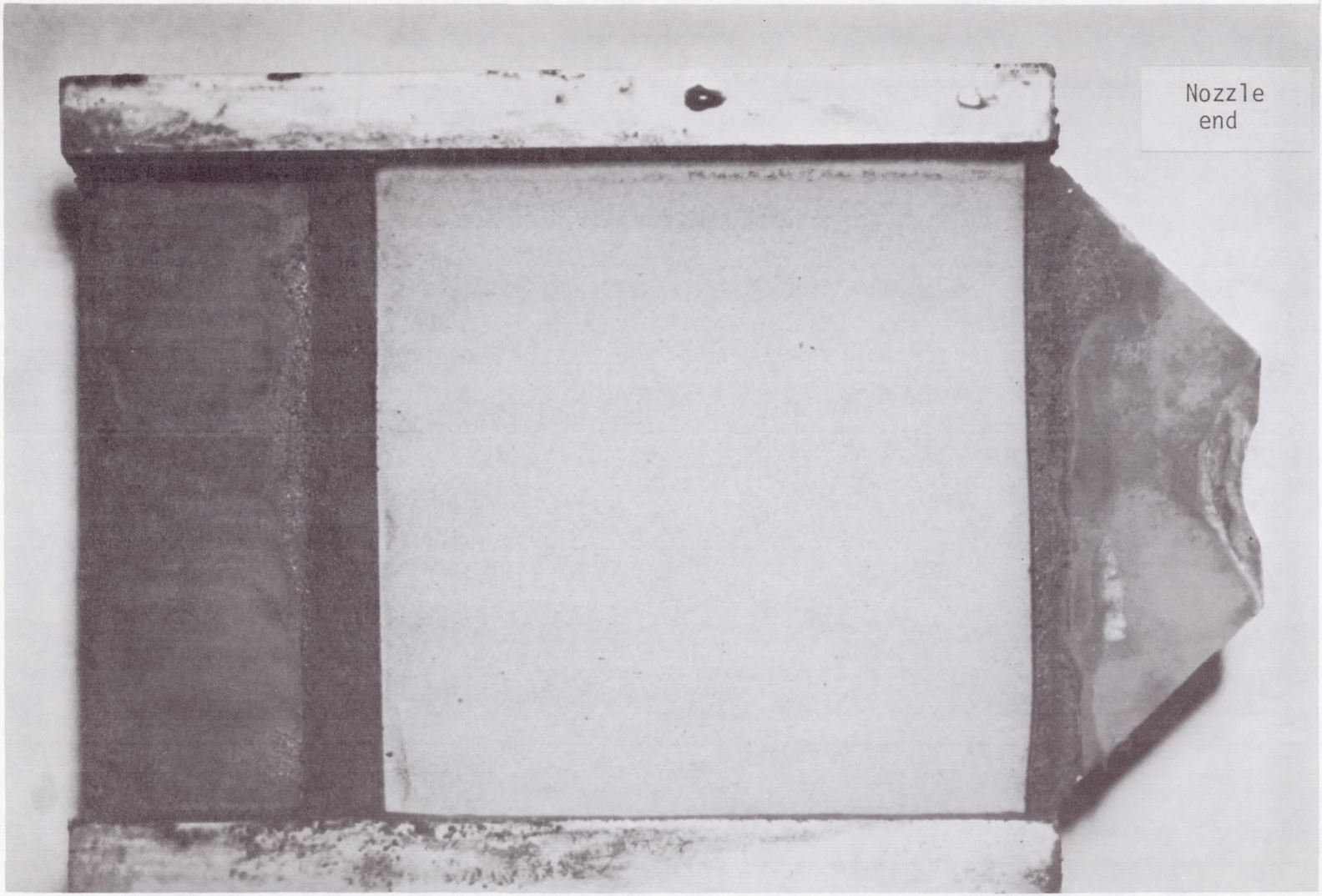

(a) 0.5 second; 0g; 90°; normal acceleration. L-68-5675

Figure 19.- Extinguished propellant.

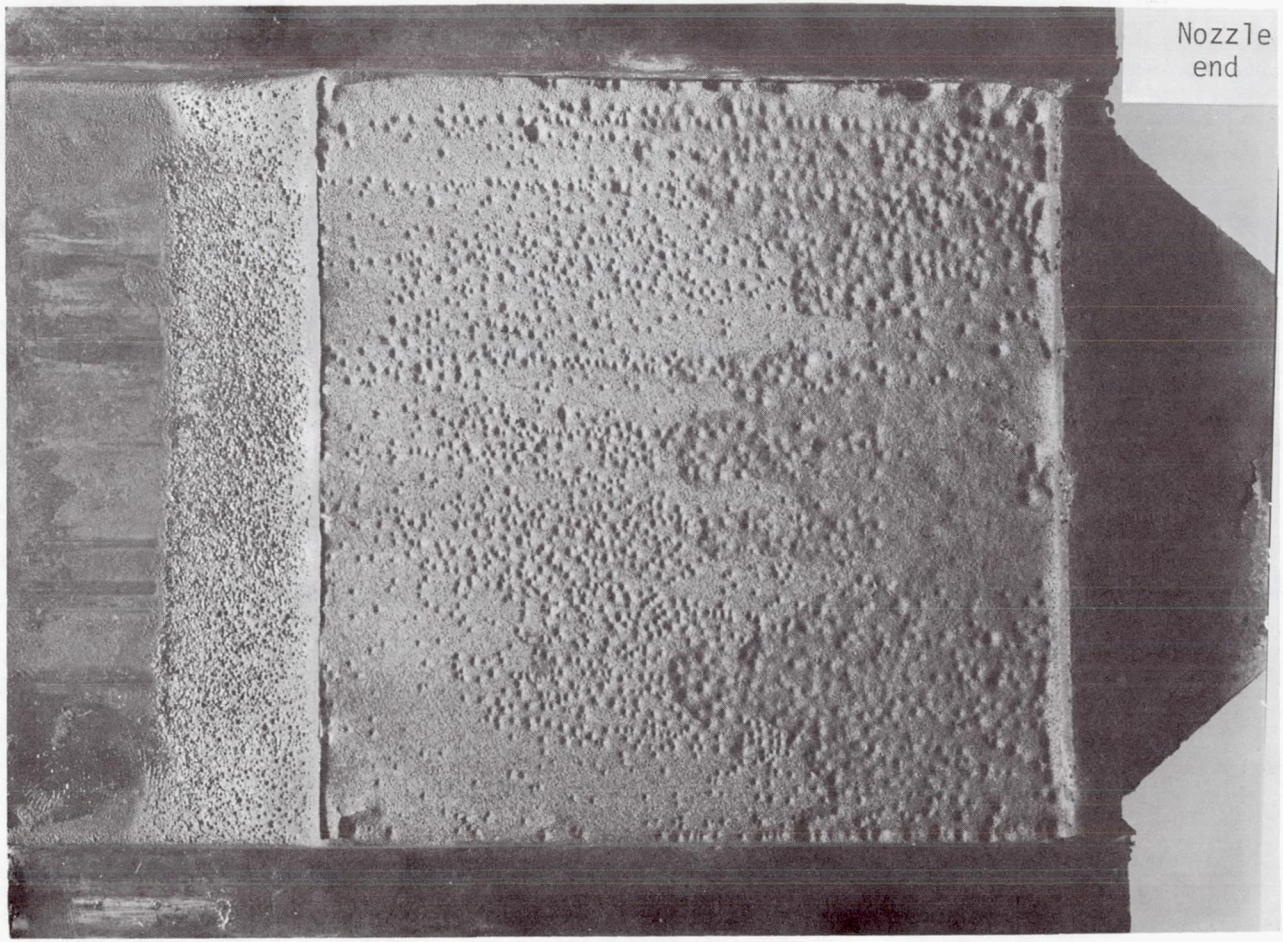

(b) 0.5 second; 100g; 90°; normal acceleration. L-68-5676

Figure 19.- Continued.

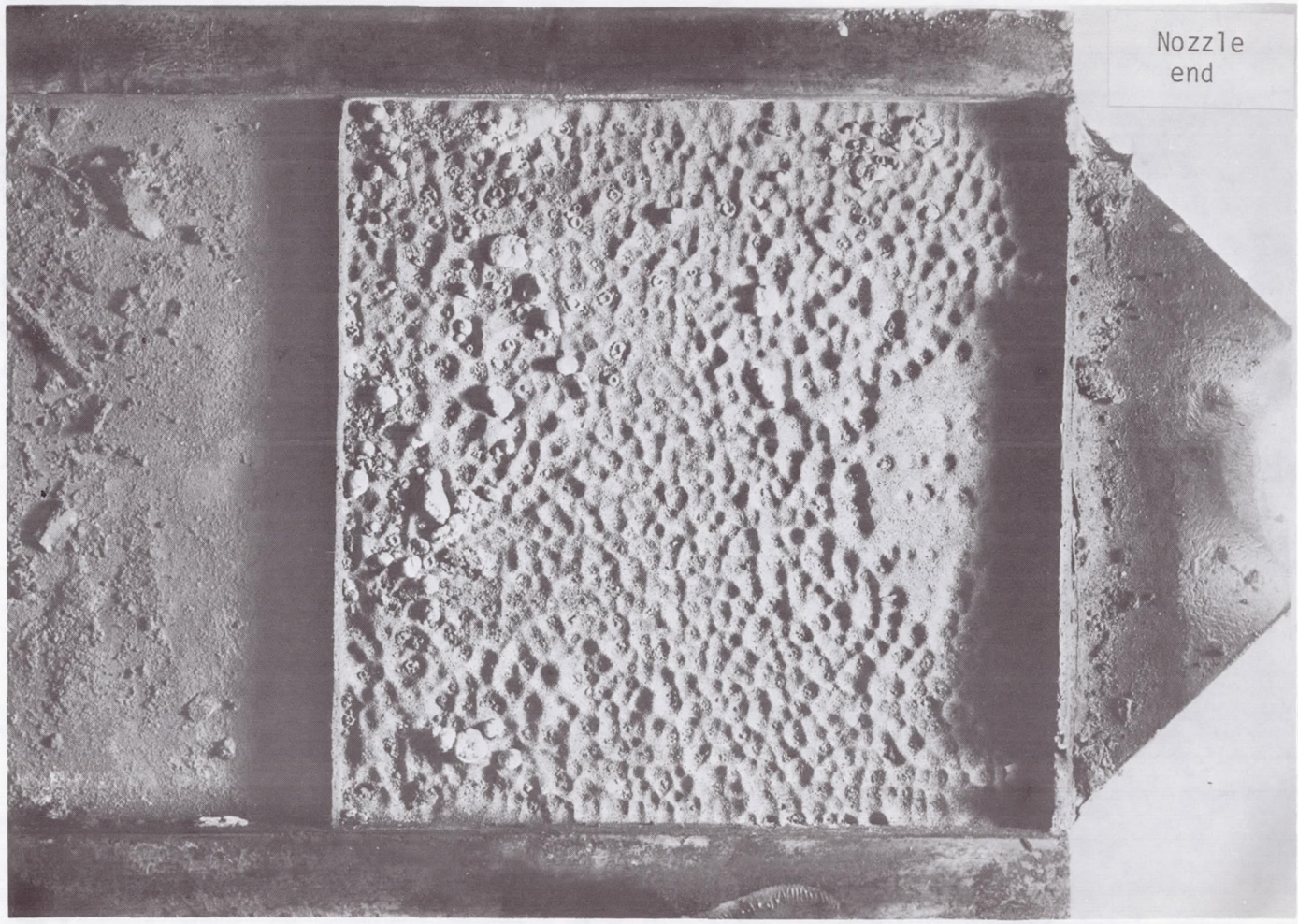

(c) 1.5 seconds; 100g; 90^{0}; normal acceleration. L-68-5677

Figure 19.- Continued.

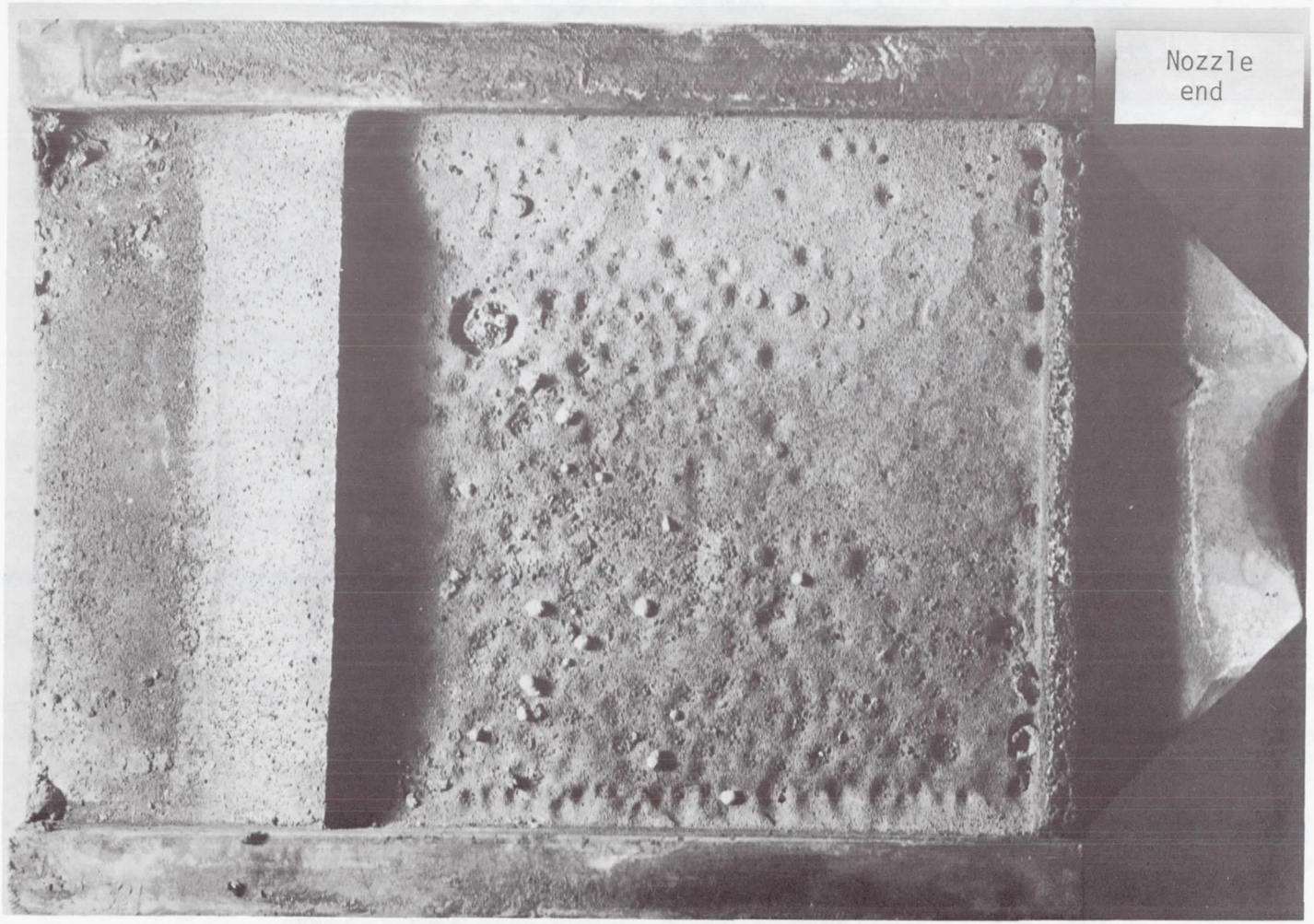

(d) 1.5 seconds; 40g; 90^{0}; normal acceleration. L-68-5678

Figure 19.- Continued.

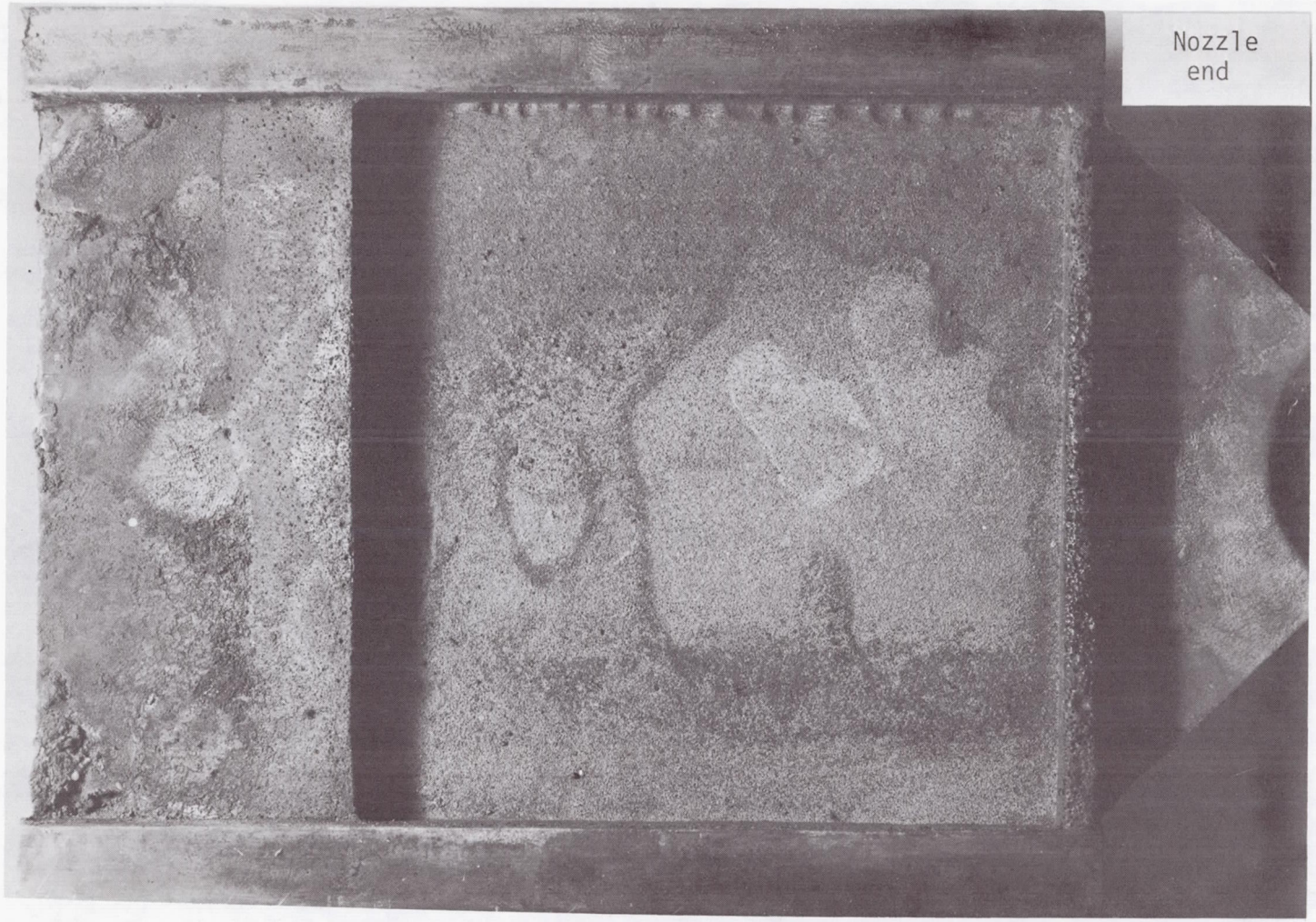

(e) 1.5 seconds; 100g; 60^{0}; normal acceleration. L-68-5679

Figure 19.- Concluded.